the Debye temperature, we can show from Eqs. (9) and (10) that the relativistic shift term in Eq. (8) is at least two orders of magnitude smaller than the isomer-shift term at these two transitions. So we have for the expected discontinuity of the shift (in velocity units)

$$(C/E_A)(\delta E_A)=C(\partial \ln E_A/\partial \ln V)_T{}^{\text{isom}}(\delta V/V). \quad (11)$$

Straight-line-segment fits were made to the data in Fig. 9 for temperatures 816°C and above. At the α-γ transition, $(\delta E_A)_{\alpha\gamma}$ was evaluated by subtracting the values for the α-phase fit at 930°C from the value of the γ-phase fit at 930°C, giving

$$(C/E_A)(\delta E_A)_{\alpha\gamma}=-(0.041\pm0.004)\text{ mm/sec}.$$

But if $(\partial \ln E_A/\partial \ln V)_T{}^{\text{isom}}$ is obtained from Eq. (9) and $\delta V/V$ is taken from the volume expansion data of Basinski *et al.*,[15] we obtain

$$C\left(\frac{\partial \ln E_A}{\partial \ln V}\right)_T^{\text{isom}}\frac{(\delta V)_{\alpha\gamma}}{V}=-(0.013\pm0.002)\text{ mm/sec},$$

which leaves a residual value of $-(0.028\pm0.005)$ mm/sec to be accounted for in the isomer-shift discontinuity at $T_{\alpha\gamma}$.

Similarly, for the γ-δ transition, $(C/E_A)(\delta E_A)_{\gamma\delta}=-(0.07\pm0.02)$ mm/sec but

$$C\left(\frac{\partial \ln E_A}{\partial \ln V}\right)\frac{(\delta V)_{\gamma\delta}}{V}=+(0.007\pm0.001)\text{ mm/sec},$$

which leaves a jump of $-(0.08\pm0.02)$ mm/sec unexplained in $(C/E_A)(\delta E_A)_{\gamma\delta}$, four times as large and of the same sign as the unexplained part of $(C/E_A)(\delta E_A)_{\alpha\gamma}$.

It is worth noting that the discontinuity in the energy shift is not only too large but also in the wrong direction to be explained by Eq. (9) at $T_{\gamma\delta}$. At the α-hcp phase transition in iron under high pressures, Pipkorn *et al.*[19] observe a similar discontinuity in the isomer shift which is several times too large to be explained by Eq. (9). They say that the large shift must be related to a difference in the band structure of the two phases and cite several mechanisms without attempting to make any calculations.

It has not been possible in the present experiment to construct a quantitative theoretical explanation of the large size of these discontinuities in the isomer shift in iron at phase changes, nor were any attempts to do this found in the literature.

PHYSICAL REVIEW VOLUME 181, NUMBER 2 10 MAY 1969

Semiclassical Theory of a High-Intensity Laser*

STIG STENHOLM† AND WILLIS E. LAMB, JR.
Department of Physics, Yale University, New Haven, Connecticut 06520
(Received 30 September 1968)

This paper extends the calculations of the semiclassical Lamb theory of a Doppler-broadened gas laser (optical maser) to arbitrary intensities for the case of single-mode operation. The coupled equations of the classical electromagnetic field and an ensemble of two-level atoms are set up, and a solution is obtained in the form of a continued fraction. This is used to compute intensity-detuning curves and atomic population inversion densities as functions of both the velocity and the position in the laser. When the laser is tuned to resonance, the velocity dependence of the inversion density shows a previously unknown fine structure consisting of a "bump" in the bottom of the hole. The calculations are compared to results obtained from a perturbation expansion in powers of the field and exact results known for atoms with zero velocity. The response of the laser output to a slow modulation and the buildup of oscillations are also discussed.

1. INTRODUCTION

THE semiclassical theory of gas lasers given by Lamb[1,2] is capable of explaining, at least qualitatively, most observed features of the operation. These include the detuning dip[3] and mode competition effects.[4] Extensions of the theory to the cases of Zeeman lasers[5] and ring lasers[6] have been given and pressure effects on the laser performance have been considered.[7] Only laser characteristics which intrinsically depend on

* Work supported by the U. S. Air Force Office of Scientific Research and the National Aeronautics and Space Administration.
† Present address: Research Institute for Theoretical Physics, University of Helsinki, Helsinki 17, Finland.
[1] W. E. Lamb, Jr., Phys. Rev. **134**, A1429 (1964).
[2] W. E. Lamb, Jr., in *Quantum Optics and Electronics*, edited by C. DeWitt, A. Blandin, and C. Cohen-Tannoudji (Gordon and Breach, Science Publishers, Inc., New York, 1965).
[3] R. A. McFarlane, W. R. Bennett, Jr., and W. E. Lamb, Jr., Appl. Phys. Letters **2**, 189 (1963); A. Szöke and A. Javan, Phys. Rev. Letters **10**, 521 (1963); Phys. Rev. **145**, 137 (1966).
[4] R. L. Fork and M. A. Pollack, Phys. Rev. **139**, A1408 (1965); J. Haisma and G. Bouwhuis, Phys. Rev. Letters **12**, 287 (1964); W. J. Witteman and J. Haisma, *ibid.* **12**, 617 (1964); W. J. Witteman, Phys. Rev. **143**, 316 (1966).
[5] R. L. Fork and M. Sargent III, Phys. Rev. **139**, A617 (1965); M. Sargent III, W. E. Lamb, Jr., and R. L. Fork, *ibid.* **164**, 436 (1967); **164**, 450 (1967); W. J. Tomlinson, M. A. Pollack, and R. L. Fork, Appl. Phys. Letters **11**, 150 (1967); W. J. Tomlinson and R. L. Fork, Phys. Rev. **164**, 466 (1967).
[6] B. L. Gyorffy and W. E. Lamb, Jr. (to be published).
[7] B. L. Gyorffy, M. Borenstein, and W. E. Lamb, Jr., Phys. Rev. **169**, 340 (1968).

the quantum-mechanical nature of light, such as threshold behavior, oscillator linewidth, and photon statistics, cannot be discussed within the framework of the semiclassical theory; a quantum-mechanical version[8] of the theory is, however, capable of treating these problems.

One limitation of the treatment in Ref. 1 is that the calculations are carried out only to third order in the electromagnetic field. This approximation is sufficient to bring in the important phenomenon of saturation but cannot be expected to have a very large region of validity. Indeed, it has been found experimentally that small deviations occur even at rather moderate amplitudes of the laser field.[9] It is then difficult to see whether the difference between observation and calculation is due to the truncation of the solution or is inherent in the formulation of the problem. Consequently, more general solutions of the semiclassical model of the laser are needed. Calculations including the fifth-order terms[10] become very cumbersome since the complexity of the expressions increases enormously and it is difficult to pursue this path to terms of very high order.

It is the purpose of this paper to consider a method of calculation which can easily be carried through for electromagnetic fields of any magnitude and which converges considerably better than a straightforward perturbation expansion in powers of the field. The result of the calculation is expressed as a continued fraction. A strong signal theory for stationary atoms was indicated in Ref. 1, but it is essential for the treatment of a gas laser to include atomic motion because some of the most important characteristics of the laser are related to the velocity distribution of the atoms. In order to treat these effects, we employ a Fourier expansion method similar to one also proposed by Lax.[11] He, however, restricted his discussion to the lowest approximation, which is equivalent to a solution obtained earlier in Ref. 1. Our method leads to successive approximations in a form suitable for numerical computations in spite of the fact that for moving atoms the ensuing Fourier series only converge asymptotically.

The Doppler shifts due to atomic motion cause the laser oscillations to be sustained only by atoms of velocity in two narrow ranges. This results in an effect termed "hole burning" by Bennett[12] and leads to a qualitative interpretation of the detuning dip. The holes are given a clear interpretation in the theory of Ref. 1 and they can be seen distinctly in the computations of the present paper. An unexpected fine structure of the hole is discovered, which cannot be explained in the approximations of Ref. 1 or by qualitative considerations such as those of Ref. 12.

Our theory can be used to calculate the response of a laser subjected to a slow modulation[9] and transients can also be considered. The recent work by Born[13] does, in fact, correspond to the use of our lowest approximation and the generalization to higher approximations is straightforward.

The calculations of this paper are restricted to the single-mode case. Sections 2 and 3 derive the basic equations of the semiclassical theory in the form used in the rest of the paper. The method of solution is presented in Sec. 4 and the lowest approximation is discussed in Sec. 5. Section 6 outlines the computer calculations which in the following sections are used to obtain various quantities of interest in a working laser. Section 7 discusses the intensity-detuning curves and their calculation. The Fourier series are discussed in Sec. 8, where we show that they are only asymptotically convergent but can be summed numerically to give the spatial distribution of the atomic population inversion. Section 9 calculates the Fourier coefficients occurring in our theory in the form of a perturbation expansion in powers of the electromagnetic field. The atomic inversion as a function of velocity is discussed in Sec. 10 and the results are compared to the results calculated from the perturbation expansion. The fine structure of the hole is also discussed in Sec. 10. Section 11 discusses adiabatic modulation and transients in the laser. Section 12 contains the conclusions of the present paper regarding the relation between the laser intensity and the excitation relative to threshold excitation. Appendices A and B show that the present work contains the known results for stationary atoms and those obtained by third-order perturbation theory.

2. ELECTROMAGNETIC FIELD

According to the theory of Ref. 1, the laser is regarded as a one-dimensional resonant cavity of length L (in the z direction). The electromagnetic field in the cavity is described classically by Maxwell's equations. We now summarize the basic results to be used later in the present paper.

The eigenfrequency for the nth cavity mode is

$$\Omega_n = cK_n = (c\pi/L)n \tag{1}$$

and the corresponding (unnormalized) eigenfunction is

$$U_n(z) = \sin K_n z . \tag{2}$$

We consider only the situation where one single mode is undergoing laser oscillations and omit the subscript n.

[8] M. Scully, W. E. Lamb, Jr., and M. J. Stephen, in *Proceedings of the Physics of Quantum Electronics Conference, San Juan, Puerto Rico, 1965*, edited by P. Kelley, B. Lax, and P. Tannenwald (McGraw-Hill Book Co., New York, 1965), p. 759; M. Scully and W. E. Lamb, Jr., Phys. Rev. Letters **16**, 852 (1966); Phys. Rev. **159**, 208 (1967); **166**, 246 (1968); and (to be published).

[9] P. T. Bolwijn, thesis, University of Utrecht, 1967 (unpublished); J. Appl. Phys. **37**, 4487 (1966); P. T. Bolwijn and C. Th.J. Alkemade, Phys. Letters **25A**, 632 (1967).

[10] K. Uehara and K. Shimoda, Japan J. Appl. Phys. **4**, 921 (1965); W. Culshaw, Phys. Rev. **164**, 329 (1967).

[11] M. Lax, *1966 Brandeis University Summer Institute in Theoretical Physics Lectures* (to be published).

[12] W. R. Bennett, Jr., Appl. Opt. Suppl. **1**, 24 (1962); **2**, 3 (1965); Phys. Rev. **126**, 580 (1962).

[13] G. K. Born (private communication) (to be published); cf. also G. K. Born, Appl. Phys. Letters **12**, 46 (1968).

The electromagnetic field equations for the case considered are

$$(\partial/\partial z)E(z,t)=-(\partial/\partial t)B(z,t),$$
$$-(\partial/\partial z)H(z,t)=J(z,t)+(\partial/\partial t)D(z,t), \tag{3}$$

with

$$B(z,t)=\mu_0 H(z,t),$$
$$D(z,t)=\epsilon_0 E(z,t)+P(z,t),$$
$$J(z,t)=\sigma E(z,t),$$

and the conductivity σ is introduced phenomenologically to represent all losses in the system.

We look for solutions of the field equations with the spatial dependence of the cavity mode

$$E(z,t)=A(t)\sin Kz \tag{4}$$

and find for $A(t)$ the equation

$$(d^2/dt^2)A(t)+(\sigma/\epsilon_0)(d/dt)A(t)+\Omega^2 A(t)$$
$$=-(1/\epsilon_0)(d^2/dt^2)P(t), \tag{5}$$

where $P(t)$ is the projection of the polarization $P(z,t)$ on the oscillating cavity mode:

$$P(t)=\frac{2}{L}\int_0^L dz\, P(z,t)\sin Kz. \tag{6}$$

The frequency of the laser oscillator is denoted by ν and all terms with a frequency deviating appreciably from it will be neglected (the "rotating wave approximation"). The electromagnetic field is assumed to have the form

$$A(t)=E(t)\cos[\nu t+\varphi(t)], \tag{7}$$

where $E(t)$ and $\varphi(t)$ vary only slowly compared to $\cos\nu t$ and $\sin\nu t$.

The polarization $P(t)$ is split up into a part in phase with the field (7) and a part with a phase difference of 90°:

$$P(t)=C(t)\cos[\nu t+\varphi(t)]+S(t)\sin[\nu t+\varphi(t)]. \tag{8}$$

The expressions (7) and (8) are substituted in (5), and small terms proportional to $\dot{C}$, $\ddot{C}$, $\dot{S}$, $\ddot{S}$, $\dot{E}$, $\dot{\varphi}$, $\dot{\varphi}\dot{E}$, $\sigma\dot{E}$, and $\sigma\dot{\varphi}E$ are neglected. The last two are small because we assume the cavity to have small losses, i.e., a large Q value,

$$Q=(\epsilon_0\nu/\sigma)\gg 1. \tag{9}$$

The working frequency of the laser is always very close to the cavity frequency Ω, so that

$$\nu+\Omega+\dot{\varphi}(t)\approx 2\nu. \tag{10}$$

We equate the coefficients of the sine and cosine terms separately and find

$$[\nu+\dot{\varphi}(t)-\Omega]E(t)=-(\nu/2\epsilon_0)C(t), \tag{11}$$
$$\dot{E}(t)+(\nu/2Q)E(t)=-(\nu/2\epsilon_0)S(t). \tag{12}$$

3. POLARIZATION OF ATOMS

The model for the active medium is an ensemble of independent atoms with an upper state a and a lower state b (see Fig. 1). These are introduced into the cavity at random times and random positions with a prescribed distribution of velocities. This is presumably a good description of the complicated pumping mechanism in a gas laser. Collisions are neglected so that the atom introduced at the position z_0 at the time t_0 with velocity v in the z direction is at a later time t situated at the position

$$z=z_0+v(t-t_0).$$

The velocity v may be large enough to take the atom through several wavelengths of the electromagnetic field before it decays to lower states with decay rates γ_a and γ_b for levels a and b, respectively. The atomic frequency $\omega=(W_a-W_b)/\hbar$ is close to the cavity frequency Ω and the interaction with the electromagnetic field induces transitions between the two levels. When more atoms are found in the upper state a than in the lower state b (population inversion), the electromagnetic field shows a tendency to increase by absorbing energy from the atoms. The atomic polarization induced by the field appears as the driving term in Maxwell's equations and sustains the oscillations. When the field obtained as a solution of these equations is equal to the field assumed in the calculation of the polarization, the solution is self-consistent.

The atomic transitions $a\leftrightarrow b$ are caused by the perturbation

$$\hbar V(z,t)=-\wp E(z,t)$$
$$=-\wp E(t)\sin[K(z_0+v(t-t_0))]\cos\nu t, \tag{13}$$

where $\wp$ is the electric dipole matrix element

$$\wp=e\langle a|x|b\rangle. \tag{14}$$

[In a steady state $\varphi(t)$ is a constant which may be set equal to zero in the rest of the paper without loss of generality.]

The time development of the elements of the density matrix ρ for one atom introduced as described above is

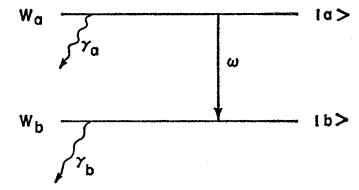

FIG. 1. The two states a and b involved in the laser transition have the energies W_a and W_b, respectively. The atomic transition $a\leftrightarrow b$ is at resonance at the frequency $\omega=(W_a-W_b)/\hbar$ and both levels are allowed to decay to lower states with the rates γ_a and γ_b, respectively.

determined by the equations

$$\begin{aligned}
\dot{\rho}_{aa} &= -\gamma_a\rho_{aa}+iV(z,t)(\rho_{ab}-\rho_{ba}),\\
\dot{\rho}_{bb} &= -\gamma_b\rho_{bb}-iV(z,t)(\rho_{ab}-\rho_{ba}),\\
\dot{\rho}_{ab} &= -\gamma_{ab}\rho_{ab}-i\omega\rho_{ab}+iV(z,t)(\rho_{aa}-\rho_{bb}),\\
\rho_{ba} &= \rho_{ab}^*,
\end{aligned} \tag{15}$$

with $\gamma_{ab}=\frac{1}{2}(\gamma_a+\gamma_b)$. Equations (15) are derived and discussed in the present context in Refs. 1 and 2. Removing the fundamental frequency from the off-diagonal elements of the density matrix by writing

$$\rho_{ab}=\rho_1 e^{-i\nu t} \tag{16}$$

and neglecting terms with the time dependence $\exp(\pm i2\nu t)$, we find

$$\begin{aligned}
\dot{\rho}_{aa} &= -\gamma_a\rho_{aa}-\tfrac{1}{2}i(\wp E/\hbar)(\rho_1-\rho_1^*)\sin Kz,\\
\dot{\rho}_{bb} &= -\gamma_b\rho_{bb}+\tfrac{1}{2}i(\wp E/\hbar)(\rho_1-\rho_1^*)\sin Kz,\\
\dot{\rho}_1 &= -\gamma_{ab}\rho_1+i(\nu-\omega)\rho_1\\
&\quad -\tfrac{1}{2}i(\wp E/\hbar)(\rho_{aa}-\rho_{bb})\sin Kz.
\end{aligned} \tag{17}$$

The polarization to be introduced into the equations for the electromagnetic field must be calculated at a point z and at a time t. We thus want to consider an ensemble of atoms arriving at z at time t, but with various histories, and sum their contributions to the macroscopic polarization. The density matrix describing this ensemble can be calculated from the results of Ref. 1, Sec. 4.

The equations of motion (17) are integrated from t_0 up to a time $\hat{t}$, not necessarily equal to t, first with the atoms introduced at z_0 and t_0 with velocity v into the state a, the density matrix $\rho(a,z_0,v,t_0,\hat{t})$ having the initial condition

$$\rho_{\alpha\beta}(a,z_0,v,t_0,t_0)=\delta_{\alpha\beta}\delta_{a\alpha}, \tag{18}$$

and then once more with the atoms introduced into the state b, i.e., the initial condition

$$\rho_{\alpha\beta}(b,z_0,v,t_0,t_0)=\delta_{\alpha\beta}\delta_{b\alpha}. \tag{19}$$

The number of atoms introduced into the state α per unit time and unit volume is denoted by $\Lambda_\alpha(z,t)$ and assumed to be independent of the velocity distribution $W(v)$, which is taken to be Maxwellian. The velocity average is postponed and consequently the following equations will contain the variables z, t, and v as fixed parameters only. We sum the contributions, at time $\hat{t}$, to the density matrix of the ensemble of all atoms arriving at z at the time t with velocity v, wherever and whenever they were introduced into the laser, including contributions from both atomic states:

$$\tilde{\rho}(z,v,t,\hat{t})=\sum_{\alpha=a,b}\int_{-\infty}^{\hat{t}}dt_0\int dz_0\,\Lambda_\alpha(z_0,t_0)\rho(\alpha,z_0,v,t_0,\hat{t})\times\delta(z-z_0-v(t-t_0)), \tag{20}$$

where the z_0 integration is over the whole length of the laser and the t_0 integration is over all times prior to $\hat{t}$.

Using (20), we can write the macroscopic polarization in the form

$$P(z,t)=\wp\int_{-\infty}^{+\infty}dv\,W(v)\times[\tilde{\rho}_{ab}(z,v,t,\hat{t})+\tilde{\rho}_{ba}(z,v,t,\hat{t})]_{\hat{t}=t}. \tag{21}$$

From (16) it follows that

$$\begin{aligned}
\rho_{ab} &= \rho_1(\cos\nu t-i\sin\nu t),\\
\rho_{ba} &= \rho_1^*(\cos\nu t+i\sin\nu t).
\end{aligned}$$

These can be introduced together with (20) into (21) to give

$$P(z,t)=\int_{-\infty}^{+\infty}dv\,W(v)[C(z,v,t,t)\cos\nu t+S(z,v,t,t)\sin\nu t], \tag{22}$$

where

$$C(z,v,t,\hat{t})=\wp\sum_{\alpha=a,b}\int_{-\infty}^{\hat{t}}dt_0\int dz_0\,\Lambda_\alpha(z_0,t_0)\delta(z-z_0-v(t-t_0))\times[\rho_1(\alpha,z_0,v,t_0,\hat{t})+\rho_1^*(\alpha,z_0,v,t_0,\hat{t})], \tag{23}$$

$$S(z,v,t,\hat{t})=i\wp\sum_{\alpha=a,b}\int_{-\infty}^{\hat{t}}dt_0\int dz_0\,\Lambda_\alpha(z_0,t_0)\delta(z-z_0-v(t-t_0))\times[\rho_1^*(\alpha,z_0,v,t_0,\hat{t})-\rho_1(\alpha,z_0,v,t_0,\hat{t})]. \tag{24}$$

Besides C and S two other functions, N and M, are important to us, i.e., the population inversion density

$$N(z,v,t,\hat{t})=\sum_{\alpha=a,b}\int_{-\infty}^{\hat{t}}dt_0\int dz_0\,\Lambda_\alpha(z_0,t_0)\delta(z-z_0-v(t-t_0))\times[\rho_{aa}(\alpha,z_0,v,t_0,\hat{t})-\rho_{bb}(\alpha,z_0,v,t_0,\hat{t})] \tag{25}$$

and the total density of active atoms

$$M(z,v,t,\hat{t})=\sum_{\alpha=a,b}\int_{-\infty}^{\hat{t}}dt_0\int dz_0\,\Lambda_\alpha(z_0,t_0)\delta(z-z_0-v(t-t_0))\times[\rho_{aa}(\alpha,z_0,v,t_0,\hat{t})+\rho_{bb}(\alpha,z_0,v,t_0,\hat{t})]. \tag{26}$$

We now proceed to derive the equations of motion for C, S, N, and M. We consider the derivatives

$$(\partial/\partial\hat{t})S(z,v,t,\hat{t})=i\wp\sum_{\alpha=a,b}\int_{-\infty}^{\hat{t}}dt_0\int dz_0\,\Lambda_\alpha(z_0,t_0)\delta(z-z_0-v(t-t_0))\times(\partial/\partial\hat{t})[\rho_1^*(\alpha,z_0,v,t_0,\hat{t})-\rho_1(\alpha,z_0,v,t_0,\hat{t})], \tag{27}$$

$$(\partial/\partial\hat{t})C(z,v,t,\hat{t})$$
$$=\wp\sum_{\alpha=a,b}\int_{-\infty}^{\hat{t}}dt_0\int dz_0\,\Lambda_\alpha(z_0,t_0)\delta(z-z_0-v(t-t_0))$$
$$\times(\partial/\partial\hat{t})[\rho_1^*(\alpha,z_0,v,t_0,\hat{t})+\rho_1(\alpha,z_0,v,t_0,\hat{t})], \quad (28)$$

$$(\partial/\partial\hat{t})N(z,v,t,\hat{t})$$
$$=\Lambda_a-\Lambda_b+\sum_{\alpha=a,b}\int_{-\infty}^{\hat{t}}dt_0\int dz_0\,\Lambda_\alpha(z_0,t_0)$$
$$\times\delta(z-z_0-v(t-t_0))(\partial/\partial\hat{t})[\rho_{aa}(\alpha,z_0,v,t_0,\hat{t})$$
$$-\rho_{bb}(\alpha,z_0,v,t_0,\hat{t})], \quad (29)$$

$$(\partial/\partial\hat{t})M(z,v,t,\hat{t})$$
$$=\Lambda_a+\Lambda_b+\sum_{\alpha=a,b}\int_{-\infty}^{\hat{t}}dt_0\int dz_0\,\Lambda_\alpha(z_0,t_0)$$
$$\times\delta(z-z_0-v(t-t_0))(\partial/\partial\hat{t})[\rho_{aa}(\alpha,z_0,v,t_0,\hat{t})$$
$$+\rho_{bb}(\alpha,z_0,v,t_0,\hat{t})]. \quad (30)$$

The terms involving Λ_a and Λ_b come from the initial conditions (18) and (19) when the derivative with respect to the upper limit of the t_0 integration is carried out. The $\hat{t}$ dependence of the expressions in square brackets can be found from Eqs. (17) when $\hat{t}$ is substituted everywhere for t.

Combining these equations, we obtain

$$(d/d\hat{t})(\rho_1^*-\rho_1)$$
$$=i(\omega-\nu)(\rho_1+\rho_1^*)-\gamma_{ab}(\rho_1^*-\rho_1)+i(\wp E/\hbar)$$
$$\times\sin[K(z_0+v(\hat{t}-t_0))](\rho_{aa}-\rho_{bb}), \quad (31)$$

$$(d/d\hat{t})(\rho_1+\rho_1^*)$$
$$=-\gamma_{ab}(\rho_1+\rho_1^*)+i(\omega-\nu)(\rho_1^*-\rho_1), \quad (32)$$

$$(d/d\hat{t})(\rho_{aa}-\rho_{bb})$$
$$=-\gamma_{ab}(\rho_{aa}-\rho_{bb})-\tfrac{1}{2}(\gamma_a-\gamma_b)(\rho_{aa}+\rho_{bb})+i(\wp E/\hbar)$$
$$\times\sin[K(z_0+v(\hat{t}-t_0))](\rho_1^*-\rho_1), \quad (33)$$

$$(d/d\hat{t})(\rho_{aa}+\rho_{bb})$$
$$=-\gamma_{ab}(\rho_{aa}+\rho_{bb})-\tfrac{1}{2}(\gamma_a-\gamma_b)(\rho_{aa}-\rho_{bb}), \quad (34)$$

where the arguments $(\alpha,z_0,v,t_0,\hat{t})$ of the elements of the density matrix ρ have been omitted. When Eqs. (31)–(34) are inserted into the equations for S, C, N, and M [(27)–(30)], we find in all integrals containing the sine function the combination

$$\sin[K(z_0+v(\hat{t}-t_0))]\delta(z-z_0-v(t-t_0))$$
$$=\sin[K(z-v(t-\hat{t}))]\delta(z-z_0-v(t-t_0)), \quad (35)$$

so that the sine function may be replaced by

$$\sin[K(z-v(t-\hat{t}))]$$

and taken outside the z_0 and t_0 integrations. The result is a set of differential equations for the physically important quantities S, C, N, and M (all functions of z, v, t, and $\hat{t}$, and also depending on laser parameters such as K, $\omega-\nu$, γ_a, γ_b, Λ_a, Λ_b, $\wp$, and E):

$$(\partial/\partial\hat{t})S=-(\omega-\nu)C-\gamma_{ab}S-(\wp^2E/\hbar)$$
$$\times\sin[K(z-v(t-\hat{t}))]N, \quad (36)$$

$$(\partial/\partial\hat{t})C=-\gamma_{ab}C+(\omega-\nu)S, \quad (37)$$

$$(\partial/\partial\hat{t})N=\Lambda_a-\Lambda_b-\gamma_{ab}N-\tfrac{1}{2}(\gamma_a-\gamma_b)M+(E/\hbar)$$
$$\times\sin[K(z-v(t-\hat{t}))]S, \quad (38)$$

$$(\partial/\partial\hat{t})M=\Lambda_a+\Lambda_b-\gamma_{ab}M-\tfrac{1}{2}(\gamma_a-\gamma_b)N. \quad (39)$$

The slowly varying excitation rates Λ_a and Λ_b still depend on $z-v(t-\hat{t})$ and $\hat{t}$ but may be evaluated at z and t. Equations (37) and (39) can be integrated immediately to express $C(z,v,t,\hat{t})$ and $M(z,v,t,\hat{t})$ in terms of $S(z,v,t,\hat{t})$ and $N(z,v,t,\hat{t})$, respectively:

$$C(z,v,t,\hat{t})=(\omega-\nu)\int_{-\infty}^{\hat{t}}S(z,v,t,t')\exp[-\gamma_{ab}(\hat{t}-t')]dt'$$
$$=(\omega-\nu)\int_0^\infty S(z,v,t,\hat{t}-\tau)\exp(-\gamma_{ab}\tau)d\tau, \quad (40)$$

$$M(z,v,t,\hat{t})=-\tfrac{1}{2}(\gamma_a-\gamma_b)\int_{-\infty}^{\hat{t}}N(z,v,t,t')$$
$$\times\exp[-\gamma_{ab}(\hat{t}-t')]dt'+(\Lambda_a+\Lambda_b)/\gamma_{ab}$$
$$=-\tfrac{1}{2}(\gamma_a-\gamma_b)\int_0^\infty N(z,v,t,\hat{t}-\tau)\exp(-\gamma_{ab}\tau)d\tau$$
$$+(\Lambda_a+\Lambda_b)/\gamma_{ab}. \quad (41)$$

These expressions may then be inserted into Eqs. (36) and (38) to yield a pair of integrodifferential equations[14] which couple only $N(z,v,t,\hat{t})$ and $S(z,v,t,\hat{t})$ to each other:

$$(\partial/\partial\hat{t})S(z,v,t,\hat{t})$$
$$=-\gamma_{ab}S(z,v,t,\hat{t})-(\omega-\nu)^2\int_0^\infty S(z,v,t,\hat{t}-\tau)$$
$$\times\exp(-\gamma_{ab}\tau)d\tau-(\wp^2E/\hbar)\sin[K(z-v(t-\hat{t}))]$$
$$\times N(z,v,t,\hat{t}), \quad (42)$$

$$(\partial/\partial\hat{t})N(z,v,t,\hat{t})$$
$$=-\gamma_{ab}N(z,v,t,\hat{t})+\tfrac{1}{4}(\gamma_a-\gamma_b)^2\int_0^\infty N(z,v,t,\hat{t}-\tau)$$
$$\times\exp(-\gamma_{ab}\tau)d\tau+(E/\hbar)\sin[K(z-v(t-\hat{t}))]$$
$$\times S(z,v,t,\hat{t})+(\gamma_b/\gamma_{ab})\Lambda_a-(\gamma_a/\gamma_{ab})\Lambda_b. \quad (43)$$

The variables (z,v,t) are introduced as parameters into the solution via their occurrence in the sine function.

[14] If $\omega=\nu$ and $\gamma_a=\gamma_b$, the equations become ordinary differential equations and an analytical solution is possible. Details of this calculation will be published later.

Since the time variables here occur only as the difference $t-\hat{t}$, the solution $N(z,v,t,\hat{t})$ and $S(z,v,t,\hat{t})$ of (42) and (43) will depend only on $(z, v, t-\hat{t})$. The functions $C(z,v,t,\hat{t})$ and $M(z,v,t,\hat{t})$ are obtained from Eqs. (40) and (41) and thus also depend on $(z, v, t-\hat{t})$. The derivation of Eqs. (42) and (43) given here makes use of the $\hat{t}$ concept introduced by Sargent, Lamb, and Fork.[15]

The projection onto the cavity mode (6) and the velocity average (21) introduces two new functions:

$$S(t-\hat{t})=\frac{2}{L}\int_0^L dz\,\sin Kz\int_{-\infty}^{+\infty} dv\,W(v)S(z,v,t,\hat{t}), \quad (44)$$

$$C(t-\hat{t})=\frac{2}{L}\int_0^L dz\,\sin Kz\int_{-\infty}^{+\infty} dz\,W(v)C(z,v,t,\hat{t}), \quad (45)$$

which, as explicitly indicated, depend on the time interval $t-\hat{t}$. Combining Eqs. (6) and (22) with (44) and (45), we obtain

$$P(t)=C(0)\cos\nu t+S(0)\sin\nu t. \quad (46)$$

Using Eq. (40), we find that the functions (44) and (45) obey the relation

$$C(t-\hat{t})=(\omega-\nu)\int_0^\infty S(t-\hat{t}+\tau)\exp(-\gamma_{ab}\tau)d\tau. \quad (47)$$

Equations (11) and (12) lead to conditions for steady-state operation when we set $\dot{E}=0$, $\dot{\varphi}=0$ and $C(0)$ is expressed in terms of $S(t)$ using (47):

$$E=-(Q/\epsilon_0)S(0), \quad (48)$$

$$(\nu-\Omega)/(\omega-\nu)=-\tfrac{1}{2}[\nu/(E\epsilon_0)]\int_0^\infty S(\tau)\times\exp(-\gamma_{ab}\tau)d\tau. \quad (49)$$

For nonmoving atoms $v=0$, and it is possible to find simple steady-state solutions of (42) and (43) by requiring that $(\partial/\partial\hat{t})S=0$ and $(\partial/\partial\hat{t})N=0$. Then N and S still depend on z and satisfy the linear equations

$$\gamma_{ab}S(z)=-[(\omega-\nu)^2/\gamma_{ab}]S(z)-(\wp^2E/\hbar)\sin(Kz)\,N(z), \quad (50)$$

$$\gamma_{ab}N(z)=\tfrac{1}{4}[(\gamma_a-\gamma_b)^2/\gamma_{ab}]N(z)+(E/\hbar)\sin(Kz)\,S(z)+(\gamma_b/\gamma_{ab})\Lambda_a-(\gamma_a/\gamma_{ab})\Lambda_b, \quad (51)$$

with solutions

$$N(z)=\bar{N}[1+2I\mathfrak{L}(\omega-\nu)\sin^2Kz]^{-1}, \quad (52)$$

$$S(z)=-(\wp^2E/\gamma_{ab}\hbar)\sin Kz\,\mathfrak{L}(\omega-\nu)N(z). \quad (53)$$

where the dimensionless intensity parameter

$$I=\tfrac{1}{2}\wp^2E^2(\gamma_a\gamma_b\hbar^2)^{-1}, \quad (54)$$

the average excitation density

$$\bar{N}=(\Lambda_a/\gamma_a)-(\Lambda_b/\gamma_b), \quad (55)$$

and the dimensionless Lorentzian

$$\mathfrak{L}(\omega-\nu)=\gamma_{ab}^2[(\omega-\nu)^2+\gamma_{ab}^2]^{-1} \quad (56)$$

have been introduced. The average excitation density $\bar{N}$ is the value that $N(z)$ would have if the electromagnetic field were equal to zero. The solution given by Eqs. (52) and (53) is also obtained in Ref. 1, Sec. 16.

4. SOLUTION WITH ATOMIC MOTION

Equations (42) and (43) are simple to solve when atomic motion is neglected, as we saw in Sec. 3. For moving atoms the solution is much more complicated. The presence of the $\hat{t}$-dependent factor

$$\sin K[z-v(t-\hat{t})]=-\tfrac{1}{2}i\exp\{iK[z-v(t-\hat{t})]\}+\text{c.c.} \quad (57)$$

in (42) and (43) introduces rapid temporal variations in the functions $S(z,v,t,\hat{t})$ and $N(z,v,t,\hat{t})$. These are eliminated in the final expressions (48) and (49) for E and ν, but their presence considerably modifies the solution.

To treat the problem with moving atoms we expand N and S in Fourier series whose frequencies are multiples of those in (57):

$$S(z,v,t,\hat{t})=-i\wp\bar{N}\sum_{n=-\infty}^{+\infty}s_n(v)\times\exp\{inK[z-v(t-\hat{t})]\}, \quad (58)$$

$$N(z,v,t,\hat{t})=\bar{N}\sum_{n=-\infty}^{+\infty}d_n(v)\exp\{inK[z-v(t-\hat{t})]\}. \quad (59)$$

(The v dependence of s_n and d_n is not written out in the following.) When the electromagnetic coupling is weak, we have $N(z,v,t,\hat{t})\approx\bar{N}$. Inserting this into Eq. (42), we see that $S(z,v,t,\hat{t})$ has components with the variations $\exp\{\pm iK[z-v(t-\hat{t})]\}$. When these are put back into Eq. (43), they cause temporal oscillations in $N(z,v,t,\hat{t})$. The process is iterated and we find that only even frequencies in the expansion of N are coupled to odd frequencies in the expansion of S, and consequently it is possible to limit the summations in (58) and (59) to odd and even values of n, respectively. The Fourier series are inserted into (42) and (43), and the coefficients of equal powers of $\exp\{iK[z-v(t-\hat{t})]\}$ are equated on the two sides of the equations. This leads to the coupled difference equations

$$\begin{aligned}&[inKv+\gamma_{ab}+(\omega-\nu)^2/(\gamma_{ab}+inKv)]s_n=\tfrac{1}{2}(\wp E/\hbar)(d_{n+1}-d_{n-1}),\\&[inKv+\gamma_{ab}-\tfrac{1}{4}(\gamma_a-\gamma_b)^2/(\gamma_{ab}+inKv)]d_n=\tfrac{1}{2}(\wp E/\hbar)(s_{n+1}-s_{n-1})+(\gamma_a\gamma_b/\gamma_{ab})\delta_{n0},\end{aligned} \quad (60)$$

which can be written

$$s_n=AD_1(n)(d_{n+1}-d_{n-1}), \quad (61a)$$

$$d_n=AD_2(n)(s_{n+1}-s_{n-1})+\delta_{n0}, \quad (61b)$$

[15] See Sargent *et al.* (Ref. 5), Sec. III.

where the amplitude

$$A\equiv I^{1/2}=\wp E(2\gamma_a\gamma_b\hbar^2)^{-1/2} \tag{54'}$$

and

$$D_1(n)=\tfrac{1}{2}(\tfrac{1}{2}\gamma_a\gamma_b)^{1/2}\{[inKv-i(\omega-\nu)+\gamma_{ab}]^{-1}+[inKv+i(\omega-\nu)+\gamma_{ab}]^{-1}\}, \tag{62}$$
$$D_2(n)=\tfrac{1}{2}(\tfrac{1}{2}\gamma_a\gamma_b)^{1/2}\{[inKv+\gamma_a]^{-1}+[inKv+\gamma_b]^{-1}\}.$$

Since d_n is different from zero only for even values of n and s_n only for odd values, we can introduce a vector with components x_n and a function $D(n)$ such that

$$\begin{aligned} &x_n=d_n, \quad D(n)=D_2(n), \quad \text{if} \quad n \text{ is even}\\ &x_n=s_n, \quad D(n)=D_1(n), \quad \text{if} \quad n \text{ is odd}. \end{aligned} \tag{63}$$

Equations (61) then correspond to the infinite system

$$x_n=AD(n)(x_{n+1}-x_{n-1})+\delta_{n0}. \tag{64}$$

Equation (64) is homogeneous for $n\neq 0$ and can be written

$$1=AD(n)[(x_{n+1}/x_n)-(x_{n-1}/x_n)], \quad n\neq 0. \tag{65}$$

For $n\geq 0$ we introduce the new unknown

$$b_n=-(x_{n+1}/x_n), \tag{66}$$

and (65) gives

$$b_{n-1}=AD(n)[1+AD(n)b_n]^{-1}. \tag{67}$$

The linear difference equation (64) of second order has been transformed into a nonlinear first-order equation. Setting $n=1$ and iterating Eq. (67), we obtain an expression for b_0 in the form of a continued fraction:

$$b_0=AD(1)/[1+ID(1)D(2)/[1+ID(2)D(3)/[1+\cdots. \tag{68}$$

For $n\leq -1$ we set

$$c_n=(x_n/x_{n+1}) \tag{69}$$

and find from (65) that

$$c_n=AD(n)[1+AD(n)c_{n-1}]^{-1}. \tag{70}$$

For $n=-1$ we find by iteration

$$c_{-1}=AD(-1)/[1+ID(-1)D(-2)/[1+ID(-2)D(-3)/[1+\cdots. \tag{71}$$

It follows from (62) that

$$D(-n)=[D(n)]^*, \tag{72}$$

and consequently

$$c_{-1}=b_0^*. \tag{73}$$

We use the definitions (66) and (69) of b_0 and c_{-1} to obtain

$$\begin{aligned} x_1&=-b_0x_0,\\ x_{-1}&=c_{-1}x_0=b_0^*x_0. \end{aligned} \tag{74}$$

The expressions above give a different solution to Eqs. (65) for $n>0$ and $n<0$. This is possible because Eq. (64) with $n=0$ is inhomogeneous and enables one to connect the two solutions (compare the situation when $v=0$, discussed in Appendix A). Using Eqs. (74) in Eq. (64) with $n=0$, we find

$$x_0=AD(0)(x_1-x_{-1})+1=-AD(0)(b_0+b_0^*)x_0+1 \tag{75}$$

and

$$x_0=[1+2AD(0)\ \mathrm{Re}b_0]^{-1}. \tag{76}$$

We introduce the real quantity

$$\begin{aligned} \Sigma&=2\gamma_{ab}(2\gamma_a\gamma_b)^{-1/2}A^{-1}\ \mathrm{Re}b_0\\ &=2\gamma_{ab}(2\gamma_a\gamma_b)^{-1/2}\\ &\quad\times\mathrm{Re}\{D(1)/[1+ID(1)D(2)/[1+\cdots\}. \end{aligned} \tag{77}$$

The dependence of Σ and b_0 on v, $\omega-\nu$, and I will be indicated in the following only when necessary for clarity. The function Σ is even in v because v and i always occur in the combination iv [see (62)] and the part of b_0 that is odd in v is thus proportional to i and eliminated in (77). Taking into account the fact that $D(0)=\gamma_{ab}(2\gamma_a\gamma_b)^{-1/2}$, we find for the needed coefficients s_1, s_{-1}, and d_0 of (58) and (59), using (63), (76), (77), and (74),

$$d_0=x_0=(1+I\Sigma)^{-1}, \tag{78}$$

$$s_1=x_1=-b_0(1+I\Sigma)^{-1}, \tag{79}$$

$$s_{-1}=x_{-1}=b_0^*(1+I\Sigma)^{-1}, \tag{80}$$

and also

$$s_1-s_{-1}=-(2\gamma_a\gamma_b)^{1/2}\gamma_{ab}^{-1}A\Sigma(1+I\Sigma)^{-1}. \tag{81}$$

The rate of convergence of the continued fraction in (77) depends on the smallness of the factors:

$$f_n=ID(n)D(n+1), \tag{82}$$

which for large values of n are

$$|f_n|=\wp^2E^2(2\hbar Kvn)^{-2}=\tfrac{1}{2}I[\gamma_a\gamma_b/(Kv)^2]n^{-2}. \tag{83}$$

For small intensities or large velocities only small values of n are needed to make (82) small. For high intensities or small velocities many terms in the continued fraction have to be included. For detunings $|\omega-\nu|\gg\gamma_{ab}$ and nonresonant values of v such that $nKv\ll|\omega-\nu|$, we find that

$$|f_n|=I|D_2(n)|[\tfrac{1}{2}\gamma_a\gamma_b(\gamma_{ab}^2+n^2K^2v^2)]^{1/2}(\omega-\nu)^{-2}, \tag{84}$$

which in many cases is small enough to justify a truncation of the continued fraction before the limit (83) for large n is reached. This fact, of course, increases the usefulness of the continued-fraction expression. The advantages of the continued fraction over a power-series expansion is demonstrated in Sec. 10.

Knowing the coefficients s_1, s_{-1}, and d_0 from (78)–(80), we can obtain all the others s_n and d_n from (64). We may then calculate $S(z,v,t,\hat{t})$ from (58). Once this is

done, $C(z,v,t,\hat{t})$ is given by (40) as

$$C(z,v,t,\hat{t}) = (\omega-\nu)\int_0^\infty S(z,v,t,\hat{t}-\tau)\exp(-\gamma_{ab}\tau)d\tau$$
$$= -i(\omega-\nu)\wp\bar{N}\sum_{n,\text{odd}} s_n\int_0^\infty \exp\{-\gamma_{ab}\tau+inK \times[z-v(t-\hat{t}+\tau)]\}d\tau$$
$$= -i(\omega-\nu)\wp\bar{N}\sum_{n,\text{odd}} s_n(\gamma_{ab}+inKv)^{-1} \times\exp\{inK[z-v(t-\hat{t})]\}. \quad (85)$$

We may now set $\hat{t}=t$ and take the mode projection (6). The sums in $S(z,v,t,\hat{t})$ and $C(z,v,t,\hat{t})$ involve the expressions

$$\frac{2}{L}\int_0^L dz\,(\sin Kz)\sum_n s_n\exp(inKz) = i(s_1-s_{-1}), \quad (86)$$

$$\frac{2}{L}\int_0^L dz\,(\sin Kz)\sum_n s_n(\gamma_{ab}+inKv)^{-1}\exp(inKz) = i[s_1(\gamma_{ab}+iKv)^{-1}-s_{-1}(\gamma_{ab}-iKv)^{-1}]. \quad (87)$$

If we introduce the velocity average with the distribution function $W(v)$ and collect the results from (44), (58), (86), (81), and (77), we find

$$S(0) = -\wp^2E\bar{N}(\hbar\gamma_{ab})^{-1}\int_{-\infty}^{+\infty} W(v)\Sigma(v) \times[1+I\Sigma(v)]^{-1}dv. \quad (88)$$

Similarly, from (45), (85), (87), and (78)-(80)

$$C(0) = -(\omega-\nu)\wp\bar{N}\int_{-\infty}^{+\infty} W(v)[b_0(v)d_0(v)(\gamma_{ab}+iKv)^{-1} + b_0^*(v)d_0(v)(\gamma_{ab}-iKv)^{-1}]dv$$
$$= -2(\omega-\nu)\wp\bar{N}\,\mathrm{Re}\int_{-\infty}^{+\infty} W(v)b_0(v)(\gamma_{ab}+iKv)^{-1} \times[1+I\Sigma(v)]^{-1}dv. \quad (89)$$

In Eqs. (88) and (89) all dependence on v is written out explicitly.

The introduction of (88) and (89) into (48) and (49) gives "amplitude" and "frequency" conditions

$$(\epsilon_0\hbar\gamma_{ab})/(Q\wp^2\bar{N}) = 2\int_0^\infty W(v)\Sigma(v,\omega-\nu,I)[1+I\Sigma(v,\omega-\nu,I)]^{-1}dv, \quad (90)$$

$$(\nu-\Omega)/(\omega-\nu) = 2\wp\bar{N}\nu\epsilon_0^{-1}\int_0^\infty W(v)\,\mathrm{Re}\{b_0(v,\omega-\nu,I)(\gamma_{ab}+iKv)^{-1} \times[1+I\Sigma(v,\omega-\nu,I)]^{-1}\}dv, \quad (91)$$

where the evenness of the integrands in v has been used to change the lower limit to zero by the introduction of a factor 2. The two equations (90) and (91) determine I and $\omega-\nu$ only in an implicit way, but in practice ν may be replaced by Ω in Eq. (90), which then determines the intensity. Better values for ν and I may then be obtained by calculating the right-hand sides of (91) and (90) in iteration.

The intensity goes to zero for threshold excitation density $\bar{N}_T$ with $\omega=\nu$ and we have

$$(\epsilon_0\gamma_{ab}\hbar)/(Q\wp^2\bar{N}_T) = 2\int_0^\infty W(v)\Sigma(v,0,0)dv \equiv 2\Sigma_0, \quad (92)$$

and the intensity equation (90) becomes

$$\bar{N}_T/\bar{N} = \Sigma_0^{-1}\int_0^\infty W(v)\Sigma(v,\omega-\nu,I) \times[1+I\Sigma(v,\omega-\nu,I)]^{-1}dv = \mathfrak{N}^{-1}, \quad (93a)$$

written in terms of the relative excitation $\mathfrak{N}$ defined by

$$\mathfrak{N} = \bar{N}/\bar{N}_T. \quad (93b)$$

5. LOWEST CONTINUED-FRACTION APPROXIMATION

In this section we shall consider the lowest approximation in the present scheme. If we set $I=0$ in (77), we find

$$\Sigma(v) = 2\gamma_{ab}(2\gamma_a\gamma_b)^{-1/2}\,\mathrm{Re}D(1) = \gamma_{ab}(2\gamma_a\gamma_b)^{-1/2} \times[D(1)+D(-1)] = \tfrac{1}{2}[\mathfrak{L}(\omega-\nu-Kv)+\mathfrak{L}(\omega-\nu+Kv)], \quad (94)$$

where (62) and (56) have been used. Equation (88) then gives

$$S(0) = -\wp^2\bar{N}E(2\gamma_{ab}\hbar)^{-1} \times\int_{-\infty}^{+\infty}[\mathfrak{L}(\omega-\nu-Kv)+\mathfrak{L}(\omega-\nu+Kv)]W(v) \times\{1+\tfrac{1}{2}I[\mathfrak{L}(\omega-\nu+Kv)+\mathfrak{L}(\omega-\nu-Kv)]\}^{-1}dv. \quad (95)$$

This result is obtained by Lamb in Ref. 1, Sec. 18, where in single-mode operation the approximation is shown to be equivalent to a rate equation approach. Hence, we will call it the "rate equation approximation" (REA) in the following.

The velocity distribution is taken to be Maxwellian:

$$W(v) = u^{-1}\pi^{-1/2}\exp(-v^2/u^2), \quad (96)$$

and the integral in (95) can be expressed in terms of the plasma dispersion function by expanding the integrand in partial fractions. In this section, however, we consider only the Doppler limit, i.e., when $Ku \gg \gamma_{ab}$. This limit is rather well achieved in many experiments and is easy to treat.

Even if the result (95) does not include the terms of third order in the electric field, coming from the I dependence of Σ in (88), it does include the third-order terms of most importance in the Doppler limit. This is shown in Appendix B.

We look at two limiting cases: (a) $|\omega-\nu|\ll\gamma_{ab}$ and (b) $|\omega-\nu|\gg\gamma_{ab}$. In case (a) only small velocities will contribute to the integral in (95) and we set $\omega=\nu$ in the Lorentzian. It then follows that the integral can be written

$$2\int_{-\infty}^{+\infty}\gamma_{ab}^2[K^2v^2+\gamma_{ab}^2(1+I)]^{-1}W(v)dv$$
$$=2\gamma_{ab}(Ku)^{-1}(1+I)^{-1/2}\pi^{-1/2}\int_{-\infty}^{+\infty}y(x^2+y^2)^{-1}$$
$$\times\exp[-x^2/(Ku)^2]dx. \quad (97)$$

The integral is equal to π in the asymptotic limit $Ku\gg y=\gamma_{ab}(1+I)^{1/2}$ and Eq. (95) becomes for case (a)

$$S=-\wp^2\bar{N}E(\hbar Ku)^{-1}\pi^{1/2}(1+I)^{-1/2}. \quad (98)$$

In case (b) we get a contribution to the integral of (95) only when $|Kv|\approx|\omega-\nu|$ and one Lorentzian in the denominator is of order $[\gamma_{ab}/(\omega-\nu)]^2$ and can be neglected. The integral can then be written

$$\int_{-\infty}^{+\infty}\gamma_{ab}^2[(\omega-\nu-Kv)^2+\gamma_{ab}^2(1+\tfrac{1}{2}I)]^{-1}W(v)dv$$
$$=(\gamma_{ab}/Ku)\pi^{1/2}(1+\tfrac{1}{2}I)^{-1/2}$$
$$\times\exp[-(\omega-\nu)^2/(Ku)^2], \quad (99)$$

in which case

$$S=-\wp^2\bar{N}E(2\hbar Ku)^{-1}\pi^{1/2}(1+\tfrac{1}{2}I)^{-1/2}$$
$$\times\exp[-(\omega-\nu)^2/(Ku)^2]. \quad (100)$$

The relations (98) and (100) were given in Ref. 1, Sec. 19, for the case $|\omega-\nu|\ll Ku$. They are valid approximations to (95) as long as

$$I\gamma_{ab}^2\ll(Ku)^2, \quad (101)$$

a condition which is rather mild in the Doppler limit. For the case without detuning, $\omega=\nu$, the approximation (94) breaks down for much smaller values of I than those violating (101). When $|\omega-\nu|\gg\gamma_{ab}$, a good approximation is obtained from (94) and consequently from (100) for a larger range of intensities (see Secs. 4 and 7).

6. NUMERICAL CALCULATIONS

The performance of a gas laser is most easily understood theoretically in the Doppler limit $Ku\gg\gamma_{ab}$ and in this limit we do not expect the general results to be very sensitive to the exact choice of decay parameters γ_a, γ_b, and γ_{ab} as long as they are all small compared to Ku. To illustrate the use of our equations we approximate the values used in Ref. 7: $\gamma_a=8.3$ MHz, $\gamma_b=18.6$ MHz, and $Ku=470$ MHz. It is convenient to scale the calculation with respect to γ_{ab} and we take

$$\gamma_a/\gamma_{ab}=0.6, \quad \gamma_b/\gamma_{ab}=1.4, \quad Ku/\gamma_{ab}=40. \quad (102)$$

Most experiments are performed under conditions corresponding to the Doppler limit, although not always to the extent indicated by (102).

A computer program was written in order to calculate the continued fraction Σ of (77) to a preassigned accuracy for varying detunings $|\omega-\nu|$ and intensities I. The calculations were performed on the Yale IBM 7090/7094 system using FORTRAN IV. The intensity-detuning curves, the atomic population difference N as a function of velocity, and the Fourier coefficients x_n can all be obtained as soon as Σ is known. Also, the spatial distribution of the atomic population inversion and the dipole moment density can be calculated. These quantities will be discussed to some extent in the following sections.

The computer program truncates the continued fraction (77) and calculates its value. Then it repeats the calculation including two more stages in the fraction and compares the real parts. If the difference is less than the desired accuracy of 0.1% the calculation is terminated. Otherwise it is continued.

The velocity average in (93) is calculated from a simple three-point Simpson rule. Since important values of the integral occur in an interval of order γ_{ab}/K around $v=|\omega-\nu|/K$ but the integration region is of order $u\gg\gamma_{ab}/K$, it is advantageous to start the integration at $v=|\omega-\nu|/K$ and go in both directions. For large values of v, the integration is stopped when the last value of the function to be averaged over velocity multiplied by the integral over the velocity distribution $W(v)$ from that point to infinity is less than 0.3% of the total integral. This presumably gives an upper limit to the error introduced by the cutoff. The integral over the range $0\leq v\leq|\omega-\nu|/K$ is stopped either at $v=0$ or at the mirror image with respect to $|\omega-\nu|/K$ of the high-velocity cutoff, whichever occurs first. The program then reduces the step length of the integration and reevaluates the integral until the result agrees with the previous one to 0.3%. The step has to be much less than γ_{ab}/K to give accurate results. Once the continued fraction is calculated, all other quantities can be obtained in a straightforward manner. The over-all accuracy of the computed results is estimated to be about 1%.

7. DETUNING CURVES

After calculating the function Σ of (77), we introduce it into (93) to find the relative excitation $\mathfrak{N}$ as a function of $|\omega-\nu|$ and I. It proves to be convenient to plot $\mathfrak{N}$ as a function of I for various fixed values of the detuning parameter $|\omega-\nu|$. The resulting curves are shown in Fig. 2. A given excitation corresponds to a horizontal line which crosses the family of curves with detunings at which the laser oscillates. The excitation necessary

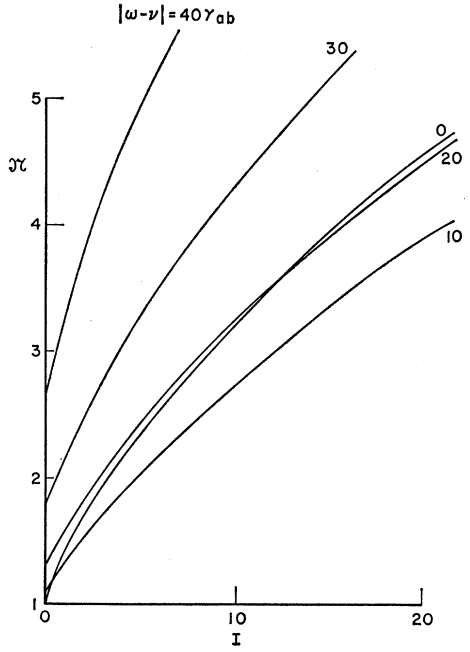

FIG. 2. Relative excitation $\mathfrak{N}$ needed to achieve a given intensity I plotted with the detuning $|\omega-\nu|$ as a parameter. The curves give a graphical representation of Eq. (93) in the text. The parameters of the laser are given in Eq. (102), in particular, $Ku=40\gamma_{ab}$.

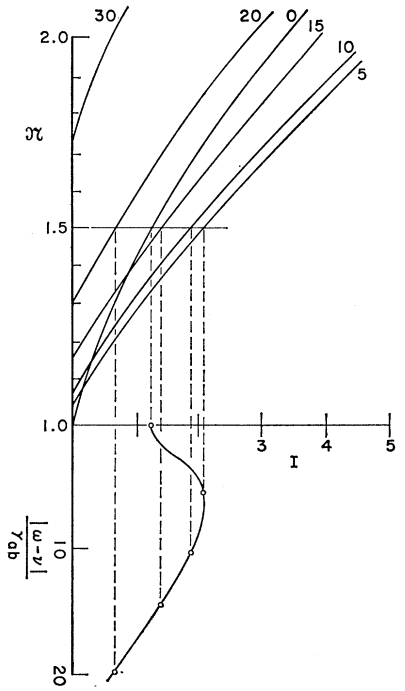

FIG. 4. A fixed relative excitation $\mathfrak{N}$ corresponds to a horizontal line in Fig. 2. Its intersections with the curves of varying detuning $|\omega-\nu|$ determine the corresponding intensities I, which then can be plotted as a function of $|\omega-\nu|$ to give the intensity-detuning curves. The construction of the curve for $\mathfrak{N}=1.5$ is shown in this figure.

to reach oscillation threshold for a given detuning is shown in Fig. 3. The intersection between the constant excitation line and the curves of Fig. 2 give the intensity-detuning curves; the construction of these is illustrated in Fig. 4. The resulting intensity-detuning curves are shown in Fig. 5, and in Fig. 6 for larger relative excitations. It is clear that the present calculations show a pronounced tuning dip for $\omega=\nu$. From Fig. 2 it is seen that when $|\omega-\nu|=\frac{1}{2}Ku$, the intensity has returned to approximately the same level as at $\omega=\nu$. For the intensity range under consideration the maximum in the curves occurs close to $|\omega-\nu|=\frac{1}{4}Ku$, moving slightly outwards for larger intensities. The curves for $\omega=\nu$ and $|\omega-\nu|=\frac{1}{4}Ku$, have been calculated out to an intensity $I\geq 200$ and the depth of the tuning dip still seems to increase monotonically. The results of this calculation can be seen in Fig. 16, which is used to discuss the intensity-excitation relations in the laser. It should be pointed out that these very large intensities are unrealistic, because single-mode operation would presumably be impossible to maintain at such high relative excitations. The details of our conclusions depend on the choice of Ku/γ_{ab}.

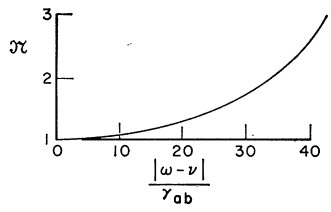

FIG. 3. Increase in relative excitation $\mathfrak{N}$ needed to reach oscillation threshold for increasing detuning of the laser $|\omega-\nu|$. The curve is obtained from the intersections between the $\mathfrak{N}$ axis and the curves in Fig. 2.

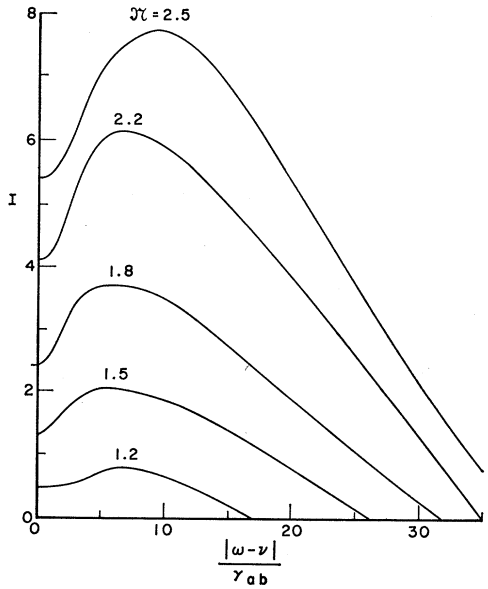

FIG. 5. Intensity curves plotted against detuning for various values of $\mathfrak{N}\leq 2.5$ obtained as illustrated in Fig. 4.

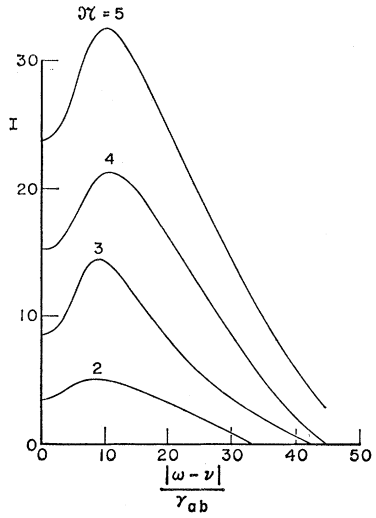

FIG. 6. Same as Fig. 5 but with $2\leq\mathfrak{N}\leq 5$. The tuning dip is distinctly seen in all cases.

8. FOURIER EXPANSION

Once s_1, s_{-1}, and d_0 are known, it is possible to calculate all Fourier coefficients from Eq. (64) in the form

$$x_{n+1}=x_{n-1}+[AD(n)]^{-1}x_n. \tag{103}$$

We set $x_1=s_1=-b_0d_0$ and find

$$\begin{aligned}
d_2&=d_0\{1-b_0[AD(1)]^{-1}\},\\
s_3&=d_0\{-b_0+[AD(2)]^{-1}-b_0[A^2D(1)D(2)]^{-1}\},\\
d_4&=d_0\{1-b_0[AD(1)]^{-1}-b_0[AD(3)]^{-1}\\
&\quad+[A^2D(2)D(3)]^{-1}-b_0[A^3D(1)D(2)D(3)]^{-1}\},
\end{aligned} \tag{104}$$

etc. It is seen that the higher Fourier coefficients bring in terms of higher inverse powers of A (the powers of A are to be counted taking into account the fact that b_0 is of first order in A).

It is possible to calculate the Fourier coefficients for very large n directly. From Eq. (62) it then follows that

$$AD(n)\sim\wp E(2i\hbar Kvn)^{-1}, \tag{105}$$

provided that $v\neq 0$. When this limiting form is inserted into (103), we find

$$x_{n+1}=x_{n-1}+2i\hbar Kv(\wp E)^{-1}nx_n. \tag{106}$$

It is easy to see that the asymptotic solution of this equation is

$$x_n=\text{const}\,[(2i\hbar Kv)/(\wp E)]^{n-1}(n-1)!, \tag{107}$$

which shows that the Fourier series (58) and (59) can at most be asymptotically convergent. We thus have a case where for $v=0$ a convergent Fourier expansion can be obtained (see Appendix A), but as soon as $v\neq 0$, the Fourier expansion diverges. Physically, however, only the first few terms in the expansion are important, since the mode projection and the velocity average suppress the rapidly oscillating z- and v-dependent higher-order terms. In Fig. 7 we show the relative magnitude of the Fourier coefficients for several values of v as computed from Eq. (103). The calculation is carried out for an intensity $I=3.2$ and resonant tuning $\omega=\nu$. The coefficients go down to $10^{-4}d_0$ before they start to grow. For small values of v, the atoms interact more strongly with the electromagnetic field and several terms in the expansion are important. For $Kv\gg\gamma_{ab}$ only the first, x_0, is of importance. Then the increase of coefficients appears earlier than for small values of v but there clearly remains a range of values of n with very small coefficients. We are thus encouraged to sum the series for the atomic population inversion density

$$N(z,v)/\bar{N}=\sum_{n,\text{even}}s_n\exp(inKz) \tag{108}$$

up to the point where the next term gives an extremely small contribution. In this way we expect to obtain an asymptotically correct series. This summation has been performed in the interval $0\leq Kz\leq\pi$ for several values of the velocity. The result is shown in Fig. 8. If the laser were not oscillating, the population inversion density would be spatially constant, normalized to unity in the figure. For this case of resonant tuning we can clearly see the saturation holes in the spatial distribu-

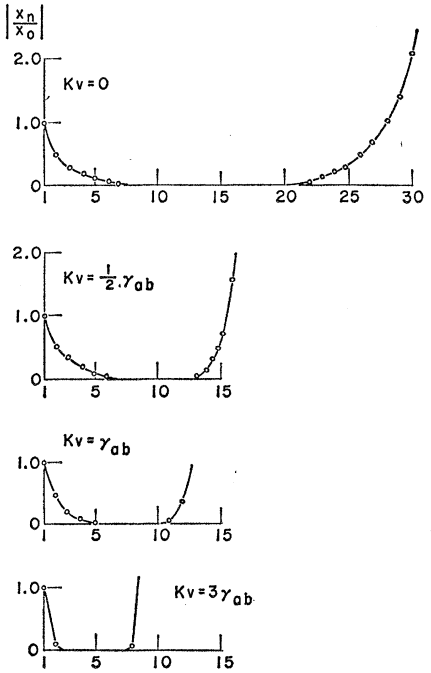

FIG. 7. Plots of Fourier coefficients. When the two coefficients x_0 and x_1 have been calculated, the following ones can be evaluated with the use of Eq. (103). The even ones occur in the expansion of N and the odd ones in S. They are complex but the absolute value of their ratio to x_0 is plotted here as a function of the position of the coefficient in the sequence $(x_0,x_1,\cdots,x_n,\cdots)$. The intensity in this picture is $I=3.2$ and the laser is tuned to resonance $\omega=\nu$. The values of the velocity are indicated in the figure.

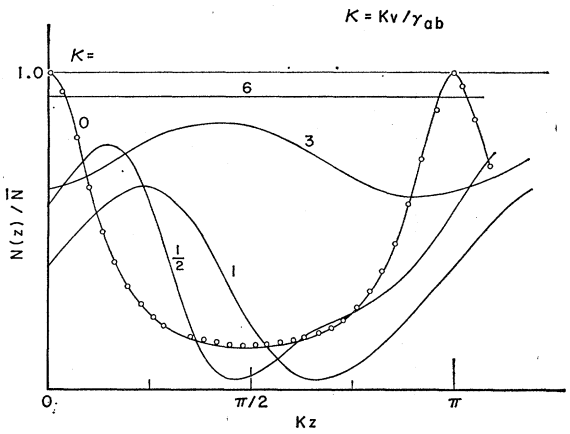

FIG. 8. Degree of saturation along the laser axis for various values of the velocity and at resonance $\omega=\nu$. The unsaturated level is here normalized to unity for all velocities. Since the laser oscillation cavity mode number is very high, this pattern is repeated many times along the laser axis. The electromagnetic field, proportional to $\sin Kz$, causes the saturation to be large near $Kz=\frac{1}{2}\pi$. In this picture the intensity is $I=3.2$. The points are exact results known for $v=0$ from Appendix A. The small disagreement between the points and the curve for $v=0$ is presumably due to truncation errors in the calculations of the Fourier series.

tion $N(z,v)$, especially for low values of v. As v increases, the holes tend to fill in, and for $v=6\gamma_{ab}/K$ we have already reached an almost uniform unsaturated distribution.

As v increases, the location of the maximum population difference is shifted along the laser axis. For example, in the case $v=\gamma_{ab}/K$, Eq. (108) becomes

$$N(z,v)/\bar{N}=0.32[1+0.93\sin(2Kz+0.31) -0.11\sin(4Kz+0.96)+\cdots]. \quad (109)$$

We also note that the 12% correction to the basic variation $\exp[\pm 2iKz]$ can be seen only as a slight asymmetry in the curve $Kv=\gamma_{ab}$ of Fig. 8. The atomic populations with $v\geq u$ are further suppressed by the velocity distribution factor $W(v)$, but this is not shown in Fig. 8.

For $v=0$ the exact solution, known from (52),

$$N(z,v)/\bar{N}=(1+2I\sin^2 Kz)^{-1}, \quad (110)$$

is indicated by points in Fig. 8. The agreement with the numerical approximation is reasonably good and suggests that the other results for $Kv\neq 0$ represent an acceptable approximation to the atomic distribution. However, we have shown in Appendix A that for $v=0$ the Fourier series converge, whereas they diverge for $v\neq 0$.

9. SERIES EXPANSION IN A

For small intensities I it is presumably possible to expand all quantities of the laser theory in a power series in $A=I^{1/2}$, the first terms of which were calculated in Ref. 1. This expansion can be obtained either from the time-dependent equations (42) and (43) (as in Ref. 1) or from the Fourier-transformed equation (64), which gives power-series expansions in A for the Fourier coefficients. The latter procedure is chosen here as the subsequent mode projection is then reduced to a triviality. The velocity average still remains to be performed.

The lowest-order approximation to a solution of (64) is clearly $x_n^{(0)}=\delta_{n0}$. Writing the general solution in the form

$$x_n=\sum_{k=0}^{+\infty} A^k x_n^{(k)}, \quad (111)$$

we find the recursion relation

$$x_n^{(k+1)}=D(n)(x_{n+1}^{(k)}-x_{n-1}^{(k)}). \quad (112)$$

In the kth order all terms $x_m^{(k)}$ with $|m|>k$ are zero. The first few nonvanishing terms are

$$\begin{aligned} k=1:&\quad x_1^{(1)}=-[x_{-1}^{(1)}]^*=-D(1);\\ k=2:&\quad x_2^{(2)}=[x_{-2}^{(2)}]^*=D(1)D(2),\\ &\quad x_0^{(2)}=-D(0)[D(1)+D(-1)], \end{aligned} \quad (113)$$

etc. Summing the series (111) on the computer allows us to calculate all the coefficients s_n and d_n to desired accuracy by going to high enough powers of A, assuming the series is convergent.

Let us, for example, look at the mean population inversion density over the length of the laser for a fixed velocity:

$$N(v)=\frac{1}{L}\int_0^L N(z,v)dz=\bar{N}d_0(v), \quad (114)$$

where (59) has been used. Using (111), we find

$$N(v)=\bar{N}\sum_{k=0}^{+\infty} A^k d_0^{(k)}. \quad (115)$$

At $v=0$ we know from Appendix A that

$$N(0)=\bar{N}(1+2I)^{-1/2}, \quad (116)$$

when $\omega=\nu$. Thus the series expansion (115) can be convergent for all values of v only if $I<0.5$. In the numerical calculations to be discussed in Sec. 10 it is found that for the particular values of I used the series did not converge in the range $0\leq Kv<\gamma_{ab}$. For large values of v the convergence is good, since the terms then decrease because $D(n)$ contains a factor $(vn)^{-1}$. The series expansion is used in Sec. 10 to check the results of the continued-fraction expansion developed earlier in this paper.

10. ATOMIC POPULATION AND HOLE BURNING

For a given detuning $|\omega-\nu|$, somewhat greater than γ_{ab}, the standing-wave electromagnetic field is in resonance with two sets of atoms traveling with

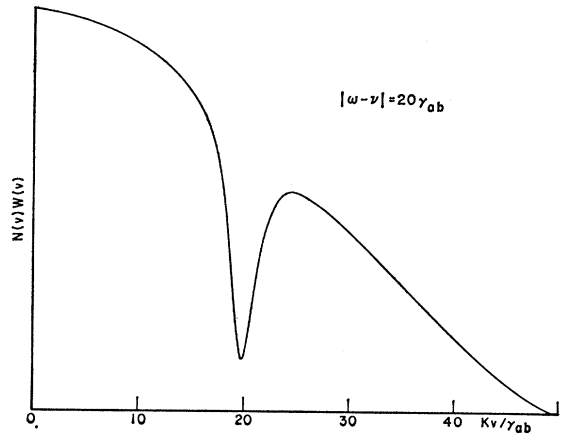

FIG. 9. Curve of the population inversion density $N(v)W(v)$ as a function of v for the detuning $|\omega-\nu|=\frac{1}{2}Ku$ showing the hole-burning effect. The parameters in this and the two following figures are $Ku=40\gamma_{ab}$, $\mathfrak{N}=2.0$. This implies that the three figures correspond to different intensities, given by the curve $\mathfrak{N}=2.0$ of Fig. 6. In this figure $I=2.87$.

velocities around $v=\pm|\omega-\nu|/K$ such that the Doppler shift compensates the detuning. The populations of the two active atomic levels are partially saturated for these velocities and $N(v)$ decreases. This phenomenon is called "hole burning" (see Ref. 12) and is seen as two dips of width approximately γ_{ab} in the velocity distribution. They can be seen when the computed values of Σ are used to plot the velocity dependence of the mean atomic population inversion (114) and (78) multiplied by the velocity distribution $W(v)$ from (96). The quantity $N(v)W(v)$ is plotted in Figs. 9–11 for different values of $|\omega-\nu|$ and the holes are clearly seen. When $|\omega-\nu|\gg Ku$, the compensation of the detuning requires atoms with such a large velocity that the factor $W(v)$ makes their density very low and laser oscillations cannot be maintained for these detunings, unless $\mathfrak{N}$ is made very large.

For $\omega\approx\nu$ the two holes at $\pm v$ merge at the position $v=0$ and use the same atoms to resonate with both the traveling waves of the electromagnetic field. These atoms are then more completely saturated than the resonant atoms would be if the two holes were a few γ_{ab}'s apart. This phenomenon, which occurs already for rather small intensities, causes the dip in the intensity-detuning curves. In Figs. 9–11 we can see how the two holes merge into one at $v=0$, but another interesting effect can also be seen. When $\omega=\nu$, the population hole takes the form of a double well. When the intensity increases, the dips move slightly outwards, while for smaller intensities they move inwards and become filled in. Only a small effect on the laser output comes from the broadening of the hole, because the two dips at the bottom are very small compared to the size of the hole.

To test the reality of the structure of the population inversion we look at the second approximation to the continued fraction (68):

$$b_0=AD(1)/[1+ID(1)D(2)], \tag{117}$$

where the functions D are given in Eq. (62) and we take $\omega=\nu$. We introduce the two parameters

$$\kappa=Kv/\gamma_{ab}, \tag{118}$$

$$\Gamma=\gamma_{ab}^2/\gamma_a\gamma_b, \tag{119}$$

and take the real part of (117). In order to see whether it is possible for the population inversion density $N(v)$ to decrease when v increases from zero, we expand (77) to second order in κ and obtain after some straightforward algebra

$$\Sigma(\kappa,I)\approx(1+\tfrac{1}{2}I)^{-1}\{1+\kappa^2(1+\tfrac{1}{2}I)^{-2}\times[(\Gamma-1)I^2+2(4\Gamma^2-\Gamma-1)I-1]\}. \tag{120}$$

When $\kappa=0$, we get $\Sigma(0,I)=(1+\frac{1}{2}I)^{-1}$, which is the lowest approximation to Eq. (A2) at $\omega=\nu$. Since the

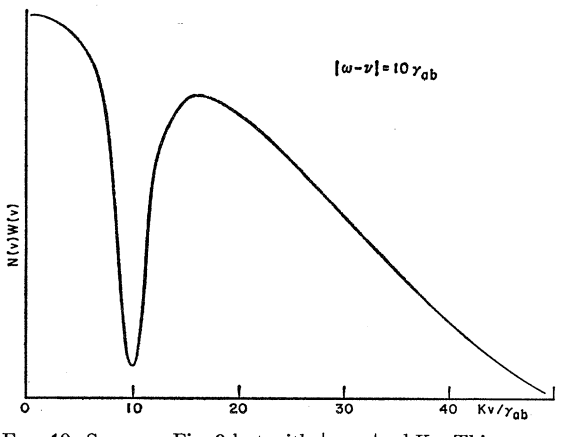

FIG. 10. Same as Fig. 9 but with $|\omega-\nu|=\frac{1}{4}Ku$. This case corresponds approximately to maximum intensity, for fixed $\mathfrak{N}$, leading to a deep and broad hole in the population inversion; here $I=4.73$.

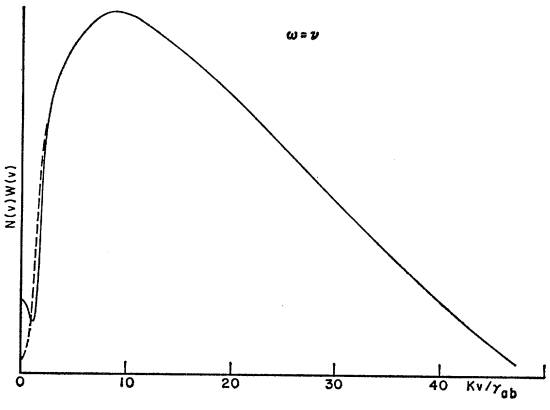

FIG. 11. Same as Figs. 9 and 10 but with $\omega=\nu$. The two holes coincide at $v=0$ and saturate these atoms strongly, leading to the occurrence of the tuning dip. A small "bump" in the bottom of the hole is clearly seen. The results of the REA of Sec. 5 are indicated as a broken line. The hole with the bump is clearly broader. In this figure $I=3.20$.

population inversion is given by Eqs. (114) and (78),

$$N(\kappa)/\bar{N}=d_0(\kappa)=[1+I\Sigma(\kappa,I)]^{-1}, \quad (121)$$

we find that an increase in $\Sigma(\kappa,I)$ for small values of κ will correspond to a decrease in $N(\kappa)$ and vice versa. Assuming the intensity I to be negligible in (120), we find

$$\Sigma(\kappa,0)=1-\kappa^2, \quad (122)$$

leading to an increase in $N(\kappa)$, i.e., no bump can occur in this approximation at $v=0$. Since (122) corresponds to the REA of Sec. 5 and the REA gives the correct results of the third-order perturbation theory of Ref. 1 in the Doppler limit (see Appendix A), we conclude that the dips in $N(\kappa)$ cannot be obtained in either REA or third-order perturbation theory. When, however, I is retained in Eq. (120), the behavior changes. The coefficients $\Gamma-1$ and $4\Gamma^2-\Gamma-1$ are always positive because $\Gamma\geq 1$. With $\Gamma=1$, i.e., $\gamma_a=\gamma_b$, we find that intensities $I>0.25$ give a positive coefficient for κ^2. Thus such intensities will give an initial decrease in $N(\kappa)$ when κ increases from zero, leading to the effect seen in Fig. 11. When Γ is larger than 1, we find a positive coefficient for even smaller intensities. Our choice of γ_a and γ_b in (102) leads to a change of sign at $I=0.14$. The approximation (117) inserted into (104) gives

$$d_2=d_0\{1-b_0[AD(1)]^{-1}\}=d_0ID(1)D(2)\times[1+ID(1)D(2)]^{-1}. \quad (123)$$

The Fourier coefficients d_2 and d_{-2} are different from zero in this approximation and cause spatial variation in the population inversion behaving as $\exp(\pm 2iKz)$ [cf. Eq. (109)] and temporal variations

$$\exp[\pm 2iKv(t-\hat{t})]$$

in the expansion (59). In the equation of motion for the function $S(z,v,t,\hat{t})$ these terms combine with the sine term (57) to contribute to the terms s_1 and s_{-1}, which support the laser oscillations. Thus spatiotemporal variations in the atomic inversion combine to give the effect shown in Eq. (120).

As a further check on the continued-fraction calculation, the case with $\omega=\nu$ is also considered using the power-series expansion of Sec. 9. In Fig. 12(a) the population inversion density of Fig. 11 is shown near $v=0$, while the dashed curve in Fig. 12(b) shows the order of the truncated power series needed for good convergence. The solid curve in Fig. 12(b) shows the number of stages in the continued fraction necessary to ensure convergence. When v approaches γ_{ab}/K, an increasingly large number of terms has to be included in the series, which finally ceases to converge, while only a gentle increase in the number of stages is required for the continued fraction even down to $v=0$. The comparison between the power series and the continued fraction in Fig. 12(a) shows a good agreement for

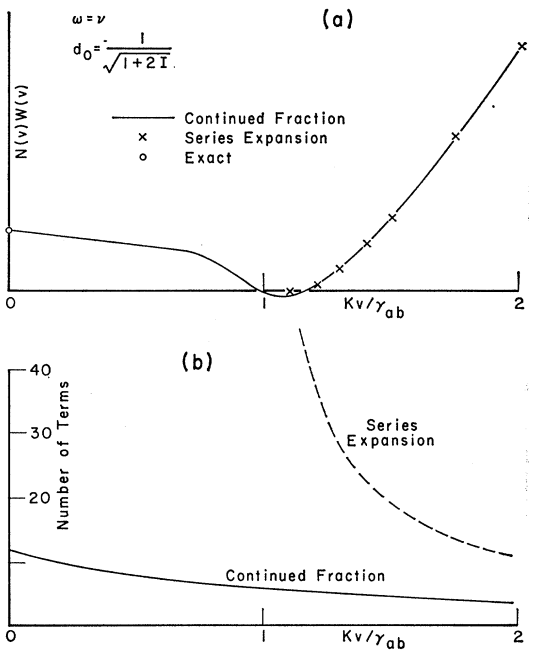

FIG. 12. (a) Detailed form of the bump in the population inversion hole of Fig. 11 obtained both from the continued-fraction calculation (solid line) and from the perturbation expansion (crosses). The value $N(0)=\bar{N}d_0$ is known exactly from Appendix A and shown as a circle in the figure. Notice that the position of the base line of this figure does not indicate the zero of the ordinate axis. (b) Number of terms needed in the series expansion compared to the number of stages in the continued-fraction expansion in the velocity range shown in (a). The intensity in this figure is $I=3.66$.

$v>\gamma_{ab}/K$. The point $v=0$, known from Appendix A, is also shown and the result agrees with the continued-fraction calculation. Since the power-series expansion gives some valid results for the inversion near $v=\gamma_{ab}/K$ which are lower than the value for $v=0$, the reality of the fine-structure phenomenon seems assured.

11. MODULATION AND TRANSIENTS IN LASERS

All equations so far have been given for steady state, but when a parameter in the laser is varied slowly, the output intensity may be expected to follow adiabatically. Such an ac modulation of the laser has been used by Bolwijn[9] to investigate the tuning dip. He finds that it is enhanced as compared to the dc dip. The third-order theory of Ref. 1 can explain the enhanced dip but the experimental results show that the ac response decreases when the laser is detuned near the point where oscillation ceases, a feature not explainable within the framework of the third-order theory. Bolwijn calls this feature in the response curve a "shoulder."

The numerical calculations of this paper can be used to obtain the adiabatic response. Bolwijn modulates Q or $\bar{N}$, but since they occur only in the combination $Q\bar{N}\propto\mathfrak{N}$ in (89), the two methods are essentially equivalent and we consider only a change in $\mathfrak{N}$. The response function $\Delta I/\Delta\mathfrak{N}$ is obtained as the inverse of

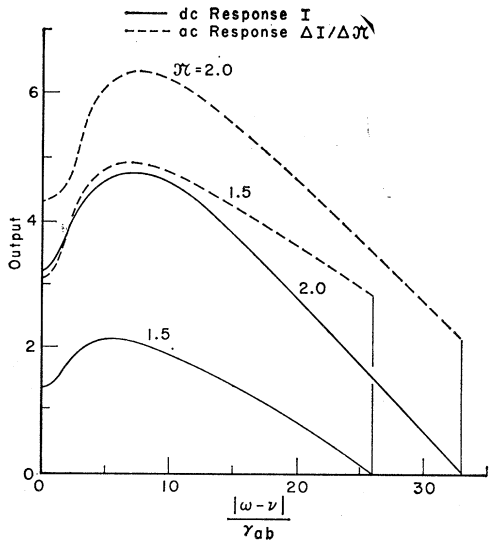

FIG. 13. Comparison between the ac and dc response of the laser intensity as a function of the detuning. For $\mathfrak{N}=1.5$ the ac curves show a clearly deeper dip.

the slope of the curves of Fig. 2 for any chosen value of $\mathfrak{N}$. Keeping $\mathfrak{N}$ constant and varying the detuning, we can directly plot the ac response curves. Looking at e.g., $\mathfrak{N}=1.5$, we find that the curve with $\omega=\nu$ starts below the curve with $|\omega-\nu|=\frac{1}{4}Ku$ but has to reach higher values of $\mathfrak{N}$ for larger intensities I, and consequently it has a larger slope $d\mathfrak{N}/dI$. The ac response $\Delta I/\Delta\mathfrak{N}$ is thus larger at $|\omega-\nu|=\frac{1}{4}Ku$ than it is at resonance. When we reach the detuning $|\omega-\nu|=\frac{1}{2}Ku$, we have a slope nearly the same as the one at $\omega=\nu$ and the shoulders start to develop. For still larger detunings (for which oscillation occurs only for larger values of $\mathfrak{N}$) the ac response becomes even smaller. As the difference between the curves at $\omega=\nu$ and $|\omega-\nu|=\frac{1}{4}Ku$ grows for increasing intensity the slopes become more alike; the dc dip now develops more fully and the ac dip decreases. For $\mathfrak{N}=2$ the two dips are approximately equal and for larger excitations the dc dip is more marked. A comparison between the ac and dc dips for various

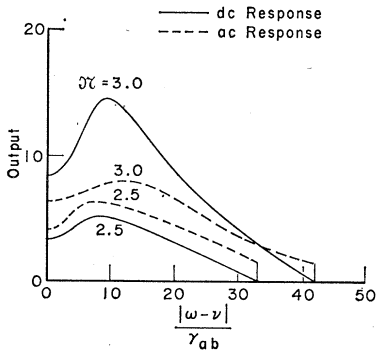

FIG. 14. Same as Fig. 13 but with larger relative excitations $\mathfrak{N}$. For $\mathfrak{N}=3.0$ the dc dip is clearly deeper than the ac one.

values of $\mathfrak{N}$ is given in Figs. 13 and 14, where the "superiority" of the ac method at $\mathfrak{N}=1.5$ and its "inferiority" at $\mathfrak{N}=3$ are clearly seen.

A qualitatively correct picture of the ac response is obtained also from the REA of Sec. 5. We have from (93)

$$\Sigma_0/\mathfrak{N}=\int_0^\infty W(v)\Sigma(v)[1+I\Sigma(v)]^{-1}dv, \qquad (124)$$

where Σ is given by (94) and thus independent of I. Taking the derivative $d\mathfrak{N}/dI$, we find

$$(\Delta I/\Delta\mathfrak{N})^{-1}(\Sigma_0/\mathfrak{N}^2)$$
$$=\int_0^\infty W(v)[\Sigma(v)]^2[1+I\Sigma(v)]^{-2}dv. \qquad (125)$$

When the detuning is varied with fixed $\mathfrak{N}$, the two equations (124) and (125) have to be solved simultaneously for I and $\Delta I/\Delta\mathfrak{N}$. This procedure can easily be performed numerically and does, indeed, show the shoulders in the ac response as a function of the detuning $|\omega-\nu|$.

The present theory can also be used to investigate other time-dependent phenomena like transients in the laser, assuming that they are slow enough. Equation (12) gives

$$dE(t)/dt=-(\nu/2Q)E(t)-(\nu/2\epsilon_0)S(t), \qquad (126)$$

and using (88), we find the integrodifferential equation for the intensity $I(t)$

$$\frac{dI}{dt}=-\left(\frac{\nu}{Q}+2\nu\wp^2\bar{N}(\hbar\epsilon_0\gamma_{ab})^{-1}\right.$$
$$\left.\times\int_0^\infty W(v)\Sigma(v,I)[1+I\Sigma(v,I)]^{-1}dv\right)I. \qquad (127)$$

Neglecting the I dependence of Σ corresponds to the REA, and calculations by Born[13] have shown that this approximation suffices to fit the experimental transients of a laser building up its oscillations from low intensity in the region $1.5\leq\mathfrak{N}\leq4$, where the steady-state intensity for $\omega=\nu$ is in the range $1.3\leq I\leq15$. The REA is expected to be a reasonably good approximation in this region, but if single-mode operation is achieved at larger intensities, the general expression (127) can be used for numerical calculations of the transients. At detunings much larger than γ_{ab} the REA is still expected to be valid even at very large intensities (see Sec. 12).

A more exact description of the modulated laser than the adiabatic one given here could be obtained by recognizing the time dependence of $\bar{N}$ in the differential equation (127). This could then be integrated numerically but the complexity is so great that we do not pursue these considerations here.

12. RELATION BETWEEN RELATIVE EXCITATION AND INTENSITY

In this section we want to summarize our results concerning the relation between intensity and relative excitation and compare the different methods of calculating them. Some conclusions regarding their range of validity will be drawn and a result suggested by the present calculations, but so far not proved, will be given.

For resonance tuning $\omega=\nu$ and in the Doppler limit the result of the third-order theory of Ref. 1 is

$$I=2(1-\mathfrak{N}^{-1}) \tag{128}$$

[see Appendix B, Eq. (B15)]. A plot of I versus $\mathfrak{N}$ starts at $\mathfrak{N}=1$ with the slope $dI/d\mathfrak{N}=2$ and has a horizontal asymptote at $I=2$. For $\mathfrak{N}\approx 1$ the third-order theory is expected to be valid and a comparison between it and the exact results calculated in this paper is shown in Fig. 15. We can see that already at $\mathfrak{N}=1.10$ the error in the output intensity is about 10%. Figure 15 also contains some points calculated from the REA to show the close agreement between the REA and the exact calculations for $\mathfrak{N}\leq 1.5$. For larger values of $\mathfrak{N}$ the deviations between the REA and the exact results are shown in Fig. 16, where it is seen that, for resonance tuning $\omega=\nu$, the output intensity obtained from the REA is about 10% below the exact result at an intensity $I=10$. Even for larger intensities the qualitative behavior of the REA is correct, in contradistinction to the third-order theory, which cannot give intensities above $I=2$. For the detuning $|\omega-\nu|=\frac{1}{4}Ku$ it is seen that the REA gives adequate accuracy for all intensities considered and it becomes still better for larger detunings.

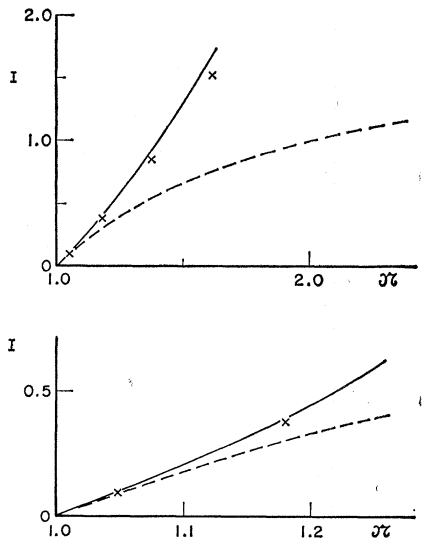

FIG. 15. Laser output intensity I at resonance $\omega=\nu$ as a function of relative excitation $\mathfrak{N}$ near threshold. The figure compares the exact calculations of this paper (solid line) to the results of the third-order theory of Ref. 1 (broken line); some points (crosses) calculated from the REA of Sec. 5 are indicated. The REA is seen to follow the exact results closely, whereas the third-order theory deviates from it appreciably already at $\mathfrak{N}=1.1$.

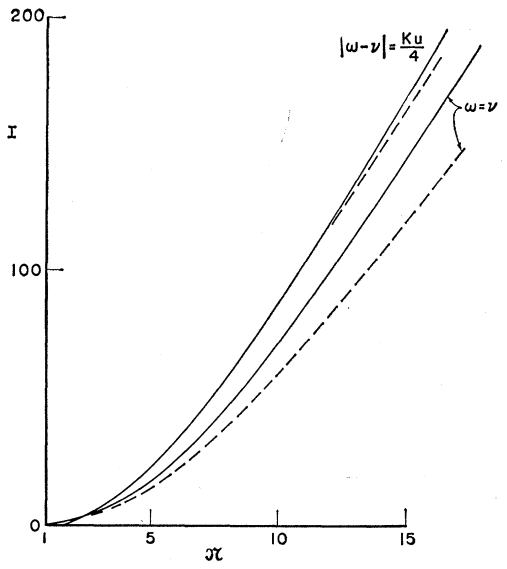

FIG. 16. Laser output intensity I at resonance $\omega=\nu$ and for $|\omega-\nu|=\frac{1}{4}Ku$, as a function of relative excitation $\mathfrak{N}$ for large values of $\mathfrak{N}$. The results of the REA are shown (broken line) and for the tuned laser $\omega=\nu$ they deviate appreciably from the exact results only for intensities larger than $I=10$ (with $\mathfrak{N}$ larger than 3.5), whereas for the detuned laser the REA gives a good approximation even for the largest intensities considered. The result of the third-order theory would have an asymptote at $I=2.0$ when $\mathfrak{N}$ goes to infinity. Since for a given $\mathfrak{N}$ the maximum intensity occurs for detunings $|\omega-\nu|\approx\frac{1}{4}Ku$, the horizontal distance between the two solid curves of this figure gives an indication of the difference between the maximum and minimum intensities of the intensity-detuning curves. The real difference cannot be smaller.

When $I\gg 1$, but the REA is still a good approximation, it follows from Eqs. (98) and (100) that $I\propto\mathfrak{N}^2$. This relation is asymptotically valid in the Doppler limit but only as long as the REA is valid. Figure 16 indicates that a region where I is a quadratic function of $\mathfrak{N}$ is present. For really large values of I the number 1 in the denominator of Eq. (95) can be neglected and we find $I\propto\mathfrak{N}$. For these values of I the REA is, however, not valid. A formal argument applied to Eq. (93) would suggest that, when $I\Sigma\gg 1$, the asymptotic result

$$I=\mathfrak{N}/\Sigma_0 \tag{129}$$

can be obtained.

However, since the behavior of Σ for large values of I is not known, the result (129) cannot be considered proved. Also, the numerical results of Fig. 16 leave the question of the existence of a linear region in the curves unsettled. The exact solution for nonmoving atoms, given in Appendix A, does, however, imply the relation (129).

APPENDIX A: CONNECTION WITH ZERO-VELOCITY THEORY

In Sec. 3 we saw that, in the case of stationary atoms, the laser problem can be easily solved exactly. In this

Appendix we show how the method developed in the main part of this paper works for nonmoving atoms. When we set $v=0$, the functions $D(n)$ of (62) take only two real values:

$$\begin{aligned} D_1&=(\tfrac{1}{2}\gamma_a\gamma_b)^{1/2}\gamma_{ab}^{-1}\mathfrak{L}(\omega-\nu), \quad n \text{ odd}.\\ D_2&=\gamma_{ab}(2\gamma_a\gamma_b)^{-1/2}, \quad n \text{ even}. \end{aligned} \tag{A1}$$

The continued fraction (77) can then be written

$$\Sigma=\mathfrak{L}(\omega-\nu)/[1+\{\tfrac{1}{2}I\mathfrak{L}(\omega-\nu)/(1+\tfrac{1}{2}I\Sigma)\}], \tag{A2}$$

which leads to a quadratic equation for Σ with the solution

$$\Sigma=I^{-1}\{[1+2I\mathfrak{L}(\omega-\nu)]^{1/2}-1\}. \tag{A3}$$

The other solution is rejected because it is negative and Σ must clearly be positive. Introduction of (A3) into (88) with the velocity average removed gives

$$S=-\wp^2\bar{N}E(\hbar\gamma_{ab}I)^{-1}\{1-[1+2I\mathfrak{L}(\omega-\nu)]^{-1/2}\}, \tag{A4}$$

which is the result given in Ref. 1, Sec. 16.

We also want to look at the difference equation (64) in the case of nonmoving atoms. We take an even value of n and find

$$d_n=AD_2(s_{n+1}-s_{n-1})+\delta_{n0}, \tag{A5}$$

and the two equations for $s_{n\pm1}$ are

$$\begin{aligned} s_{n+1}&=AD_1(d_{n+2}-d_n),\\ s_{n-1}&=AD_1(d_n-d_{n-2}). \end{aligned} \tag{A6}$$

Substituting these into (A5), we obtain

$$d_n=A^2D_1D_2(d_{n+2}-2d_n+d_{n-2})+\delta_{n0}. \tag{A7}$$

This difference equation has a solution

$$d_n=d_0r^{|n|}, \tag{A8}$$

where r is a root of the characteristic equation

$$1=ID_1D_2(r^2-2+r^{-2}). \tag{A9}$$

We note that

$$ID_1D_2=\tfrac{1}{2}I\mathfrak{L}(\omega-\nu). \tag{A10}$$

If we want the quantity (A8) to go to zero for large values of $|n|$, only the real root of (A9) which is smaller than one,

$$r^2=[I\mathfrak{L}(\omega-\nu)]^{-1}\{1+I\mathfrak{L}(\omega-\nu)-[1+2I\mathfrak{L}(\omega-\nu)]^{1/2}\}, \tag{A11}$$

can be used. For $n=0$, Eq. (A7) gives

$$d_0=d_0[\tfrac{1}{2}I\mathfrak{L}(\omega-\nu)][r^2-2+r^2]+1 \tag{A12}$$

or

$$d_0[1+(1-r^2)I\mathfrak{L}(\omega-\nu)]^{-1}=[1+2I\mathfrak{L}(\omega-\nu)]^{-1/2}, \tag{A13}$$

where Eq. (A11) has been used.

The coefficients d_n are now known and can be used in Eq. (58) to obtain the spatial distribution of the population inversion

$$\begin{aligned} N(z)&=\bar{N}\sum_{n=-\infty}^{+\infty}d_{2n}e^{2inKz}\\ &=\bar{N}d_0[1+\sum_{n=1}^{\infty}(r^2e^{2iKz})^n+\text{c.c.}]\\ &=\bar{N}d_0(1-r^4)(1+r^4-2r^2\cos 2Kz)^{-1}. \end{aligned} \tag{A14}$$

From (A9) it follows that

$$1+r^4=2[I\mathfrak{L}(\omega-\nu)]^{-1}[1+I\mathfrak{L}(\omega-\nu)]r^2, \tag{A15}$$

$$1-r^4=2r^2[I\mathfrak{L}(\omega-\nu)]^{-1}[1+(1-r^2)I\mathfrak{L}(\omega-\nu)], \tag{A16}$$

and using (A15) in (A14), we have

$$N(z)=\bar{N}d_0I\mathfrak{L}(\omega-\nu)(1-r^4)\times\{2r^2[1+2I\mathfrak{L}(\omega-\nu)\sin^2Kz]\}^{-1}. \tag{A17}$$

Introducing d_0 from (A13) and using the relation (A16), we obtain the correct expression for $N(z)$ as given by (52).

When all d_n are known, the coefficients s_n can be obtained from

$$s_n=AD_1(d_{n+1}-d_{n-1})=AD_1d_0(r^{|n+1|}-r^{|n-1|}). \tag{A18}$$

Setting $n=\pm1$, we obtain

$$s_{+1}=-s_{-1}=AD_1(r^2-1)d_0, \tag{A19}$$

which, together with (74) and (77), may be used to determine Σ in agreement with (A3). Once all coefficients s_n are known, Eq. (59) can be used to obtain $S(z)$ as given in (53) using the same algebraic steps as in (A14).

APPENDIX B: CONNECTION WITH THIRD-ORDER THEORY

In this Appendix we are going to show that the REA of Sec. 5 contains the result of the third-order theory of Ref. 1 in the Doppler limit $Ku\gg\gamma_{ab}$.

Introducing a notation for the velocity average

$$\langle f\rangle\equiv\int_{-\infty}^{+\infty}W(v)f(v)dv \tag{B1}$$

we can write Eq. (88)

$$\begin{aligned} S&=-\wp^2E\bar{N}(\hbar\gamma_{ab})^{-1}\langle\Sigma(1+I\Sigma)^{-1}\rangle\\ &\approx-\wp^2E\bar{N}(\hbar\gamma_{ab})^{-1}[\langle\Sigma\rangle-I\langle\Sigma^2\rangle], \end{aligned} \tag{B2}$$

where Σ is given by the REA expression (94) of Sec. 5. In the general case the integrals in (B2) lead to plasma dispersion functions but in the Doppler limit all velocity averages can be performed analytically. Thus

we have

$$\langle\Sigma\rangle=\int_{-\infty}^{+\infty}W(v)\mathfrak{L}(\omega-\nu+Kv)dv$$
$$=\pi^{1/2}(\gamma_{ab}/Ku)\exp[-(\omega-\nu)^2/(Ku)^2], \quad \text{(B3)}$$

whereas the term $\langle\Sigma^2\rangle$ contains several averages:

$$\langle\Sigma^2\rangle=\tfrac{1}{4}\{\langle[\mathfrak{L}(\omega-\nu-Kv)]^2\rangle+\langle[\mathfrak{L}(\omega-\nu+Kv)]^2\rangle$$
$$+2\langle\mathfrak{L}(\omega-\nu-Kv)\mathfrak{L}(\omega-\nu+Kv)\rangle\}. \quad \text{(B4)}$$

The first two terms give the same contribution:

$$\langle\mathfrak{L}^2\rangle=\pi^{-1/2}(Ku)^{-1}\int_{-\infty}^{+\infty}\gamma_{ab}{}^4[(\omega-\nu-x)^2+\gamma_{ab}{}^2]^{-2}$$
$$\times\exp[-x^2/(Ku)^2]dx$$
$$=\pi^{-1/2}(\gamma_{ab}{}^2/Ku)\exp[-(\omega-\nu)^2/(Ku)^2]$$
$$\times\int_{-\infty}^{+\infty}\gamma_{ab}{}^2(x^2+\gamma_{ab}{}^2)^{-2}dx$$
$$=\pi^{1/2}(2Ku)^{-1}\gamma_{ab}\exp[-(\omega-\nu)^2/(Ku)^2], \quad \text{(B5)}$$

since the square of the Lorentzian has a sharp peak, much narrower than the Gaussian.

We introduce the function

$$\Theta(\omega-\nu)=2(\pi\gamma_{ab})^{-1}\int_{-\infty}^{+\infty}\mathfrak{L}(\omega-\nu+x)\mathfrak{L}(\omega-\nu-x)$$
$$\times\exp[-x^2/(Ku)^2]dx. \quad \text{(B6)}$$

We consider the two limiting cases (a) $|\omega-\nu|\ll Ku$ and (b) $|\omega-\nu|\gg\gamma_{ab}$. In the Doppler limit, $Ku\gg\gamma_{ab}$, these two cases cover all possible situations. In case (a) the peaks of the two Lorentzians both fall in the region where the exponential is almost a constant and can be approximated by one. We have

$$\int_{-\infty}^{+\infty}\mathfrak{L}(x+\omega-\nu)\mathfrak{L}(x-\omega+\nu)dx=\tfrac{1}{2}\pi\gamma_{ab}\mathfrak{L}(\omega-\nu), \quad \text{(B7)}$$

giving for (B6)

$$\Theta(\omega-\nu)=\mathfrak{L}(\omega-\nu), \quad \text{for} \quad |\omega-\nu|\ll Ku. \quad \text{(B8)}$$

In case (b) the two peaks of the Lorentzians are far apart and one Lorentzian can be regarded as slowly varying over the peak of the other. We obtain

$$\int_{-\infty}^{+\infty}\mathfrak{L}(x+\omega-\nu)\mathfrak{L}(x-\omega+\nu)\exp[-x^2/(Ku)^2]dx$$
$$=\exp[-(\omega-\nu)^2/(Ku)^2]$$
$$\times\left(\mathfrak{L}(2\omega-2\nu)\int_{-\infty}^{+\infty}\mathfrak{L}(x-\omega+\nu)dx\right.$$
$$\left.+\mathfrak{L}(2\nu-2\omega)\int_{-\infty}^{+\infty}\mathfrak{L}(x+\omega-\nu)dx\right)$$
$$=\tfrac{1}{2}\pi\gamma_{ab}\exp[-(\omega-\nu)^2/(Ku)^2]4\mathfrak{L}(2\omega-2\nu). \quad \text{(B9)}$$

Inserting (B9) into (B6), we obtain

$$\Theta(\omega-\nu)=\exp[-(\omega-\nu)^2/(Ku)^2]4\mathfrak{L}(2\omega-2\nu),$$
$$\text{for} \quad |\omega-\nu|\gg\gamma_{ab}. \quad \text{(B10)}$$

Collecting the results (B3)–(B6) into (B2), we get

$$S=-\wp^2E\bar{N}(\hbar\gamma_{ab})^{-1}\exp[-(\omega-\nu)^2/(Ku)^2]\pi^{1/2}(\gamma_{ab}/Ku)$$
$$\times\{1-\tfrac{1}{4}I[1+\exp((\omega-\nu)^2/(Ku)^2)\Theta(\omega-\nu)]\}, \quad \text{(B11)}$$

which, inserted into (12), gives

$$(\hbar\epsilon_0\gamma_{ab})/(Q\wp^2\bar{N})=\pi^{1/2}(\gamma_{ab}/Ku)\exp[-(\omega-\nu)^2/(Ku)^2]$$
$$\times\{1-\tfrac{1}{4}I[1+\exp((\omega-\nu)^2/(Ku)^2)\Theta(\omega-\nu)]\}. \quad \text{(B12)}$$

When I and $\omega-\nu$ are equal to zero, we find the threshold excitation

$$(\hbar\epsilon_0\gamma_{ab})/(Q\wp^2\bar{N}_T)=\pi^{1/2}(\gamma_{ab}/Ku), \quad \text{(B13)}$$

giving

$$\mathfrak{N}=\bar{N}/\bar{N}_T=\exp[(\omega-\nu)^2/(Ku)^2]$$
$$\times\{1-\tfrac{1}{4}I[1+\exp((\omega-\nu)^2/(Ku)^2)\Theta(\omega-\nu)]\}^{-1} \quad \text{(B14)}$$

or, equivalently,

$$I=4\{1-\mathfrak{N}^{-1}\exp[(\omega-\nu)^2/(Ku)^2]\}$$
$$\times\{1+\exp[(\omega-\nu)^2/(Ku)^2]\Theta(\omega-\nu)\}^{-1}. \quad \text{(B15)}$$

In case (a) it follows that $\exp[(\omega-\nu)^2/(Ku)^2]\approx 1$ and in case (b) that $4\mathfrak{L}(2\omega-2\nu)\approx[\gamma_{ab}/(\omega-\nu)]^2\approx\mathfrak{L}(\omega-\nu)$. As either case (a) or case (b) is realized, a good approximation to (B8) and (B10) is given by

$$\Theta(\omega-\nu)=\exp[-(\omega-\nu)^2/(Ku)^2]\mathfrak{L}(\omega-\nu), \quad \text{(B16)}$$

which, inserted into (B15), leads to the denominator $1+\mathfrak{L}(\omega-\nu)$ as given in Ref. 1. The exponential in the numerator agrees with the form found in Ref. 5.